Mathematical modelling of the agr operon in Staphylococcus aureus

Jabbari, S.; King, J.R.; Koerber, A.J.; Williams, P.

DOI:
10.1007/s00285-009-0291-6

Document Version
Peer reviewed version

Citation for published version (Harvard):
Jabbari, S, King, JR, Koerber, AJ & Williams, P 2010, 'Mathematical modelling of the agr operon in Staphylococcus aureus', *Journal of Mathematical Biology*, vol. 61, no. 1, pp. 17-54.
https://doi.org/10.1007/s00285-009-0291-6

Journal of Mathematical Biology manuscript No.
(will be inserted by the editor)

Mathematical modelling of the *agr* operon in *Staphylococcus aureus*

Sara Jabbari · John R. King · Adrian J. Koerber · Paul Williams

Received: date / Accepted: date

The final publication is available at http://link.springer.com/article/10.1007/s00285-009-0291-6

Abstract *Staphylococcus aureus* is a pathogenic bacterium that utilises quorum sensing (QS), a cell-to-cell signalling mechanism, to enhance its ability to cause disease. QS allows the bacteria to monitor their surroundings and the size of their population, and *S. aureus* makes use of this to regulate the production of virulence factors. Here we describe a mathematical model of this QS system and perform a detailed time-dependent asymptotic analysis in order to clarify the roles of the distinct interactions that make up the QS process, demonstrating which reactions dominate the behaviour of the system at various timepoints. We couple this analysis with numerical simulations and are thus able to gain insight into how a large population of *S. aureus* shifts from a relatively harmless state to a highly virulent one, focussing on the need for the three distinct phases which form the feedback loop of this particular QS system.

Keywords *Staphylococcus aureus* · Quorum sensing · Mathematical modelling · Asymptotic analysis · Two component systems

Mathematics Subject Classification (2000) 34E05 · 92B05 · 37N25

Sara Jabbari (✉), John R. King
Division of Theoretical Mechanics, School of Mathematical Sciences, University of Nottingham, Nottingham, NG7 2RD, UK
E-mail: sara.jabbari@nottingham.ac.uk

Adrian J. Koerber
School of Mathematical Sciences, University of Adelaide, SA 5005, Australia

Paul Williams
Centre for Biomolecular Sciences, University of Nottingham, Nottingham, NG7 2RD, UK

1 Introduction

1.1 *Staphylococcus aureus*

Staphylococcus aureus is an opportunistic and invasive pathogen capable of promoting disease in almost any tissue of the human body [24]. While it forms part of the natural flora in a large number of people without causing any harm, *S. aureus* can cause a broad spectrum of infections, ranging from minor ailments such as superficial infections, boils and subcutaneous abscesses, to much more serious ones, for example pneumonia, endocarditis (inflammation of the heart valves), osteomyelitis (inflammation of bone and bone marrow), sepsis (infection of the blood stream), septic arthritis and toxic shock syndrome [5, 17, 24, 37].

One increasingly important factor motivating the study of this pathogenic bacterium is its ability to develop resistance to antibiotics previously used successfully in the treatment of staphylococcal infections. Methicillin-resistant *S. aureus* (MRSA) strains are multi-antibiotic resistant and are a leading cause of hospital-acquired infections. They have become increasingly difficult to treat, especially as certain strains have also developed resistance to vancomycin, one of the last therapeutic resorts for fighting *S. aureus* infection [13, 29]. In contrast to hospital-acquired MRSA strains, community-acquired (CA-MRSA) strains are much more virulent and can cause disease in healthy individuals [8]. Consequently *S. aureus* infections are the cause of much morbidity and mortality and are becoming extremely difficult to treat using conventional antibiotic therapy. New targets for the development of anti-staphylococcal agents are urgently required. In this context, attenuating the pathogenicity (the ability of one organism to cause disease in another) of *S. aureus* by inhibiting the ability of the bacterium to produce virulence factors (i.e. products that specifically allow bacteria to cause disease) offers such a target. In particular, *S. aureus* employs a cell-to-cell communication system termed ‘quorum sensing’ (QS) to control virulence gene expression. By inhibiting QS, it should be possible to prevent infection.

1.2 Gene expression and quorum sensing

In both eukaryotic and prokaryotic cells, most genes are not expressed (i.e. transcribed into mRNA and then translated into proteins) constitutively but are tightly regulated. For example, genes which code for the production of virulence factors are expressed only under particular environmental conditions such as those encountered within host tissues. The transcription of individual genes is switched ‘on’ or ‘off’ by gene regulatory proteins which bind to specific DNA sequences (namely the promoter/operator region(s) found upstream of the gene) and either activate or inhibit transcription.

S. aureus employs QS to regulate the expression of specific genes. QS depends on the synthesis of small molecules (often referred to as pheromones or autoinducers) that are both produced and detected by the bacterial cells. As the bacterial population density increases, so does the concentration of QS signal molecules (indeed, if the QS system has positive feedback the synthesis of these molecules should also increase).

This is often viewed as being associated with a critical threshold concentration of bacterial cells being reached, thus activating a target sensor or response regulator, so facilitating the expression of QS-dependent genes. However, the interpretation of such behaviour for our model will be somewhat different given that the population size is assumed to be already at or above this threshold level. Instead, we will see that the process can be understood as the density of the QS signal molecule becoming sufficiently high, rather than the population itself. This could be pertinent when, for example, a population of cells enters a new environment so that the concentration of the QS signal molecule is influenced by diffusivity within that environment, in addition to the size of the population. This is more closely linked to the more recent view that QS can in fact be a mechanism for bacteria to recognise their surroundings rather than simply detect their population size [30] (and could thus instead be referred to as 'diffusion sensing'), i.e. the concentration of signal molecule will depend upon the medium in which the bacteria reside as much as the number of bacteria producing the molecule (for a mathematical discussion of this see [25]). A more appropriate term for this cell-signalling system is perhaps 'efficiency sensing' [12] which encapsulates both of these ideas.

It is evident therefore that QS can be used for multiple purposes. For example, *S. aureus* employs QS to regulate the production of virulence factors [17,37]. In the context of infection, it has been suggested that, once inside the body, *S. aureus* coordinates the deployment of virulence factors with bacterial cell population size through QS so as to delay alerting the immune system until there are sufficient numbers of bacteria present which are capable of overwhelming the host defences [32], corresponding to the conventional interpretation of QS. On the other hand, *S. aureus* uses QS in endosome escape whereby a single bacterium can become internalised within a host cell. QS signal molecule accumulation will occur, causing production of the virulence factors allowing for endosome escape, so that here the signalling system is really being used for 'diffusion sensing'. Other uses of QS by diverse bacterial species include DNA uptake or exchange (transformation and conjugation), bioluminescence, secondary metabolite (e.g. antibiotic) production, swimming and swarming motility and biofilm (accumulation of bacteria on a surface where the micro-organism is enmeshed in a 'slime' matrix) development [3,4].

1.3 The *agr* operon

In *S. aureus*, QS is performed by the *agr* operon (see, for example, [10] or [26]) which consists of two transcription units (termed *agrBDCA* and RNAIII respectively) that are driven by regulatory proteins which bind to promoters termed P2 and P3, permitting RNA polymerase to transcribe the DNA into mRNA, prior to translation of this *agr* mRNA into proteins. The P2 transcript consists of four genes which are transcribed and translated to give four proteins (AgrB, AgrD, AgrC and AgrA), see Figure 1. AgrB is a transmembrane protein which processes the AgrD protein to generate a QS signal molecule which, in the case of the staphylococci, is a small modified peptide called an AIP (autoinducing peptide). The AIP is secreted into the external environment where it is detected by a receptor protein (AgrC) present on the bacterial cell

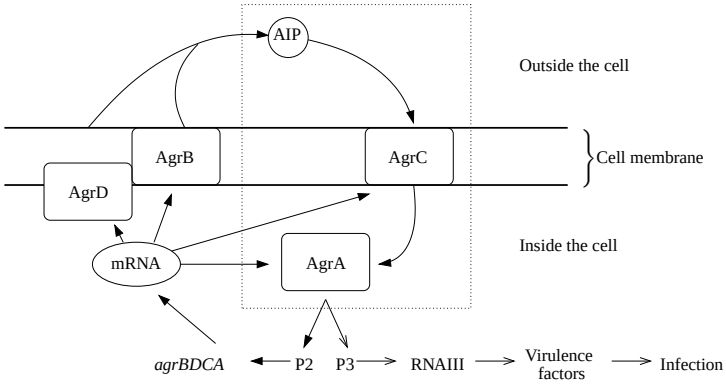

Fig. 1 A schematic representation of the *agr* feedback loop. The arrows with a filled head illustrate the positive feedback loop. This loop is unusual in that every cytoplasmic (as well as the extracellular) component of the loop is up-regulated, rather than simply the signal, which is in principle all that is required. The dotted box encloses the elements of the TCS. In Figure 2 we describe a generic TCS.

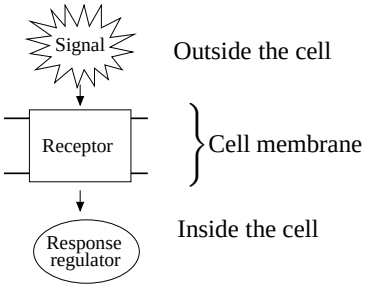

Fig. 2 A schematic representation of a generic TCS. The receptor protein can detect the presence of a specific signal and activate the response regulator which lies within the cell. For the *agr* operon AIP is the signal, AgrC the receptor and AgrA the response regulator.

surface. AIP binding to AgrC induces a phosphorylation/dephosphorylation cascade which results in the activation of AgrA, a DNA-binding protein which interacts with both the P2 and P3 promoters. AgrA and AgrC are, respectively, the response regulator and sensor kinase of a two-component system (TCS). This type of signal recognition mechanism is common throughout the bacterial kingdom, see Figure 2. Although the precise details of the AgrC and AgrA phosphorylation/dephosphorylation reactions occurring following AIP binding to AgrC are not known, in most classical TCSs the detection of the cognate signal by the sensor kinase results in autophosphorylation followed by transfer of the phosphate to the response regulator protein. The phosphorylated response regulator usually has a higher affinity for the DNA binding site than the unphosphorylated form and is therefore able to alter regulation of the target gene(s) [35]. This also seems to be the case for AgrA: see [19], where the purified phosphorylated AgrA protein is shown to bind to both the P2 and the P3 promoter with a higher affinity than the unphosphorylated form. In this paper we therefore assume that AgrA and AgrC form a classical TCS but in [15] we explore the possibility that a less conventional phosphorylation cascade may hold, whereby either AgrA or

AgrC can be constitutively phosphorylated (it is suggested in [26] that this may be possible).

On binding to the P2 promoter, AgrA upregulates the transcription of the *agr* mRNA which will be translated into each of the four Agr proteins. Thus the *agr* system is subject to positive feedback in that AIPs are generated which in turn drive the production of further AIP synthesis. This is usual in QS systems as it allows a cell to switch quickly between two states. It is noteworthy, however, that all the other components of the feedback system are also subject to upregulation and our model allows us to shed some light onto why this may be the case.

The *agr*-P3 transcript gives rise to an un-translated regulatory RNA termed RNAIII and also to a protein toxin, δ-haemolysin. RNAIII is the intracellular effector of the *agr* system which acts by upregulating transcription of many extracellular protein genes while downregulating the cell wall colonisation factor genes. Thus the cell can use the AIP concentration to coordinate virulence gene expression with cell density. This means that it should be possible to prevent *S. aureus* infections by inhibiting AIP-dependent QS by blocking either AIP synthesis or AIP action or by destroying the AIP as it accumulates extracellularly (see [3,4,28]). Interestingly, the study of *agr* systems in different *S. aureus* strains has already highlighted the potential for QS inhibition through blockade of AgrC activation. *S. aureus* strains can be divided into four groups (I to IV) depending on the structure of the AIP produced; group I strains are activated by the group I AIP but are inhibited by the AIPs made by *S. aureus* strains belonging to groups II, III or IV [22]. Indeed, [22] demonstrates that, in mice, *S. aureus* skin abscess infections caused by a strain producing AIP-I can be prevented by coadministering a group II AIP. Since the AIPs are amenable to laboratory synthesis it is possible to design inhibitors based on the AIP structure which bind to AgrC and can inhibit all *S. aureus agr* groups [23]. Such peptides need to be able to bind to the AIP-binding site on AgrC without activating the kinase and so block binding of the native (and hence activating) AIP. This would ensure that the bacterial cell remains in the QS down-regulated state.

1.4 Mathematical models of QS

Most QS models produced so far have been mathematical models of the slightly simpler Gram-negative *lux*-system (here the signal molecule is produced within the cell and is freely diffusible across the cell membrane, so that only two elements are required to complete the system: a signal synthase and a signal receptor) or its homologues, see for example [2,6,7,16,34]. To our knowledge, only two focus on QS in *S. aureus* (which is Gram-positive): Koerber *et al.* [20] model endosome escape, as described in §1.2, at the cellular level, while Gustafsson *et al.* [11] investigate the TCS of the *agr* operon (which is taken to be of a classical form) and the influence of the regulatory protein SarA on the basal transcription of the operon. The latter is more akin to the current paper as the modelling is performed at the sub-cellular level. However in [11] the TCS is treated in isolation in the sense that the AIP concentration is taken to be a parameter of the model, so that the full feedback circuit contained within the QS loop is not considered; by contrast, we include the complete

circuit shown in Figure 1, calculating the AIP level as part of the solution. By incorporating the full circuit, we aim to shed light in particular on the implications of the *agr* operon leading to multiple network elements being up-regulated. Alongside numerical simulations we will perform an asymptotic analysis of the time-dependent model in order to characterise its behaviour. This analysis will both demonstrate how a population of *S. aureus* shifts from a relatively harmless state to a highly virulent one and provide simpler models which can be used to extend this study. For inhibitor therapy to have a future in combatting staphylococcal infections, it is crucial that we gain a full understanding of how the *agr* operon works and this model is well suited to studying the effects of inhibitors; this generalisation will be addressed elsewhere.

2 Formulation

2.1 Dimensional model

We follow [14] in using a modelling approach similar to that employed by Dockery and Keener [6] in their model of virulence-related QS in *P. aeruginosa*, whereby we shall formulate a system of ordinary differential equations representing the intracellular components of the full *agr* operon. A key variable in our model is $P(t)$, which represents the proportion of cells with a bound *agr* promoter. Roughly speaking, this will be equivalent to the proportion of *agr* up-regulated cells and we will henceforth refer to P in this way, making the proportion of down-regulated cells $1-P(t)$.

In order to build the model we adopt the following assumptions.

- The bacteria are in a well-mixed environment, so spatial dependencies can be ignored, and the population size is constant (i.e. birth rate matches death and/or removal rate) and large enough to make a continuum model appropriate. These are conditions which are most similar to those of a chemostat, thus making it plausible that, to an extent, our results could be tested experimentally for possible validation and calculation of parameter values.
- *agr* mRNA is produced at some basal rate in a down-regulated population and its average rate of transcription increases linearly with the average level of upregulation in the population, $P(t)$.
- Since each molecule of this mRNA contains all the information required for the translation of all four Agr proteins, the same numbers of each of these are produced, i.e. we assume that on each pass a ribosome translates the entire strand of mRNA. We also assume there to be a plentiful supply of ribosomes within the cells since they are required for translation of all proteins, not only those involved in QS. We do not therefore need to track the concentration of ribosomes and can take the rates of translation of each of the proteins to be the same, and proportional to the concentration of *agr* mRNA.
- The levels of proteins and mRNA inside the cells are limited by natural degradation and through dilution, proteins having a relatively low rate of degradation. Bacterial cells grow until they undergo binary fission to produce two daughter cells of equal size. Each daughter receives a copy of the chromosome and sufficient numbers of all the different chemicals required for survival. We assume that

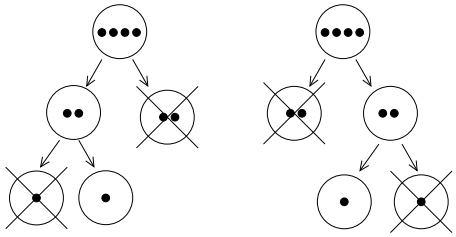

Fig. 3 Bacterial cells reproduce through binary fission, producing two daughter cells. The contents of the parent cell are divided between the daughter cells. Here death rate matches birth rate, as in our model, so the original contents of the cells (showed schematically as filled circles) are reduced through dilution.

all the contents of the parent cell are divided equally between the two daughter cells. Through this dilution process the number of proteins in each cell would, in the absence of protein production, be reduced as time goes on (see Figure 3). We assume that the contents of a dead cell are degraded and have no effect on the remaining cells. The dilution rate, r, can be calculated as $ln2/t_d$ where t_d is the time it takes for one *S. aureus* generation to undergo binary fission. We define $\delta_X = \lambda_X + r$ (see Table 1) for all intracellular concentrations X.

- Housekeeping phosphatases are able to dephosphorylate AgrA at a rate μ.
- After membrane-anchored AgrD has been (post-translationally) modified into AIP (by AgrB) we can ignore what remains of the AgrD protein as it has no further effect on the QS loop and will eventually be lost through dilution or metabolism.
- Receptor-bound AIP can unbind spontaneously, at rate γ.
- When an AIP binds to a receptor, i.e. to AgrC, the latter autophosphorylates. To simplify the system we will assume that this process is sufficiently fast that it in effect happens as soon as the AIP binds to the receptor. When the receptor transfers its phosphate to the AgrA protein (at a rate ϕ) it is free to autophosphorylate again, and the phosphorylated AgrA is able to bind to the promoter site of the DNA and increase mRNA production.
- There is a plentiful supply of SarA proteins so that, unlike in [11], we do not take into consideration their specific effect upon AgrA binding to the promoter sites.

The resulting equations are, for conciseness, shown only in Figure 4; see Tables 1 and 2 for definitions of the parameters and variables. Notice that taking the equation governing $P(t)$ to be quasi-steady would give us Michaelis-Menten kinetics for mRNA transcription, as is often done in modelling of this kind. However, we shall see that $P(t)$ is among the slower evolving variables and we accordingly retain the full dynamic balance.

We take the initial conditions of the system to be the steady state which would arise were no AIP produced ($k = 0$), i.e. a totally down-regulated state, so QS has no effect on the cells and all protein levels are controlled by translation, transcription, degradation and dilution. This could be reproducible in a chemostat experiment through manipulation of AIP synthesis, i.e. by bringing the *agr* operon under the control of an inducible promoter. As a reflection of bacteria in nature it might be interpreted as a large population of cells in which the *agr* system is suppressed by an-

Table 1 Definitions of the parameters.

Parameter	Rate constant for	Units
m	basal production of mRNA	molecules cells^{-1} s^{-1}
ν	mRNA transcription	molecules cells^{-1} s^{-1}
κ	protein translation	s^{-1}
α_T, α_R	AgrB and AgrC taken up into cell membrane	s^{-1}
α_S	AgrD anchors to cell membrane	s^{-1}
λ_X	natural degradation of variable $X(t)$	s^{-1}
r	dilution through cell division	s^{-1}
δ_X	degradation and dilution ($\delta_X = \lambda_X + r$)	s^{-1}
k	AIP production from AgrD, mediated by AgrB	molecules^{-1} cm^3 s^{-1}
β	binding of AIP to AgrC	molecules^{-1} cm^3 s^{-1}
γ	separation of AIP from AgrC	s^{-1}
ϕ	activation of AgrA by AIP-bound AgrC	molecules^{-1} cm^3 s^{-1}
μ	dephosphorylation of AgrA by phosphatases	s^{-1}
b	binding of the promoter site	molecules^{-1} cells s^{-1}
u	unbinding of the promoter site	s^{-1}
N	total number of bacteria per unit volume	cells cm^{-3}

Table 2 Definitions of the variables.

Variable	Concentration of	Units
M	mRNA	molecules cm^{-3}
A, B, C, D	cytoplasmic AgrA, AgrB, AgrC, AgrD	molecules cm^{-3}
T, R	transmembrane AgrB, AgrC	molecules cm^{-3}
S	anchored AgrD	molecules cm^{-3}
a	free AIP	molecules cm^{-3}
R^*	AIP-bound receptor	molecules cm^{-3}
A_P	phosphorylated AgrA	molecules cm^{-3}
P	proportion of cells that is up-regulated	-

other of the many gene regulation networks involved in cellular regulation, before this latter mechanism is switched off, through some environmental or metabolic change, to allow *agr* upregulation to begin. Using such initial conditions allows us to monitor how a large population of bacteria can shift into an up-regulated state as AIP levels increase. Hence we take the following initial conditions (which are the steady states of the equations in Figure 4 with $k = 0$)

$$
\begin{aligned}
&a(0) = R^*(0) = A_P(0) = P(0) = 0,\\
&M(0) = \frac{Nm}{\delta_M}, \qquad A(0) = \frac{N\kappa m}{\delta_M \delta_A}, \qquad B(0) = \frac{N\kappa m}{\delta_M(\alpha_T + \delta_B)},\\
&C(0) = \frac{N\kappa m}{\delta_M(\alpha_R + \delta_C)}, \quad D(0) = \frac{N\kappa m}{\delta_M(\alpha_S + \delta_D)}, \quad T(0) = \frac{N\alpha_T \kappa m}{\delta_M \delta_T(\alpha_T + \delta_B)},\\
&R(0) = \frac{N\alpha_R \kappa m}{\delta_M \delta_R(\alpha_R + \delta_C)}, \; S(0) = \frac{N\alpha_S \kappa m}{\delta_M \delta_S(\alpha_S + \delta_D)}.
\end{aligned}
\tag{1}
$$

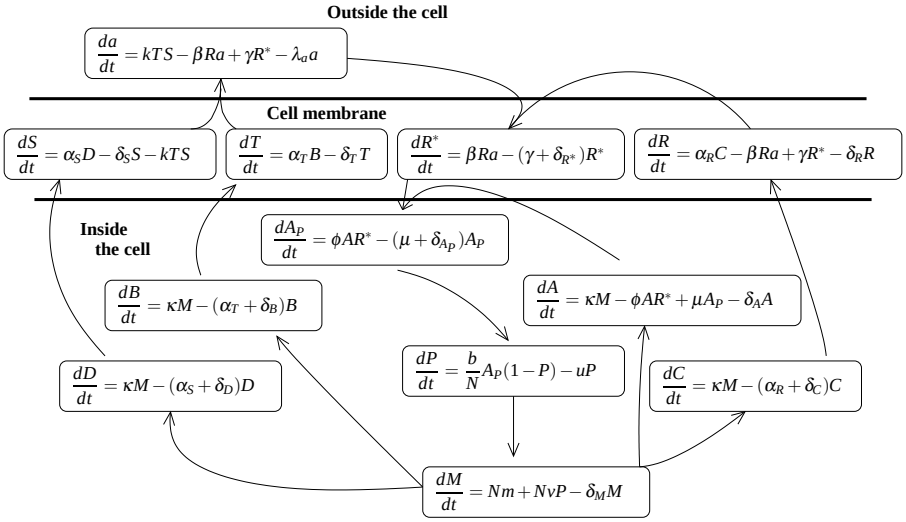

Fig. 4 A schematic representation of the complete model for the *agr* circuit with a classical TCS. See Tables 1 and 2 for definitions of parameters and variables. The dimensionless version of this model is shown in Figure 5.

2.2 Nondimensional model

We nondimensionalise the relevant[1] variables using (1), i.e. we set

$$M' = \frac{\delta_M}{Nm}M, \quad A' = \frac{\delta_M \delta_A}{N\kappa m}A, \quad X' = \frac{\delta_M(\alpha_Y + \delta_X)}{N\kappa m}X, \quad Y' = \frac{\delta_M \delta_Y(\alpha_Y + \delta_X)}{N\alpha_Y \kappa m}Y, \tag{2}$$

for $X = B,C,D$ and $Y = T,R,S$ respectively. The remaining scalings are

$$a' = \frac{\beta\phi bN\alpha_R\kappa^2 m^2}{{\delta_M}^5\delta_A\delta_R(\alpha_R+\delta_C)}a, \quad {R^*}' = \frac{\phi b\kappa m}{{\delta_M}^3\delta_A}R^*, \quad {A_P}' = \frac{b}{N\delta_M}A_P, \quad \tau = \delta_M t, \tag{3}$$

P already being dimensionless. Time is thus scaled with δ_M, the rate of mRNA degradation while the others are chosen to simplify the corresponding equations as much as possible, i.e. they are chosen to set the coefficients of basal mRNA transcription, AIP-receptor binding, AgrA activation and phosphorylated AgrA binding to the promoter site in certain equations to unity. The following dimensional parameters emerge:

$$\lambda_X' = \frac{\delta_X}{\delta_M} \quad \text{for} \quad X = A,T,R,S,R^*,A_P, \tag{4}$$

$$\alpha_{X,Y}' = \frac{\alpha_Y + \delta_X}{\delta_M} \quad \text{for} \quad (X,Y) = (B,T),(C,R) \text{ or } (D,S), \tag{5}$$

[1] Namely mRNA and all unphosphorylated proteins, since these would be the only non-zero variables in a totally down-regulated cell.

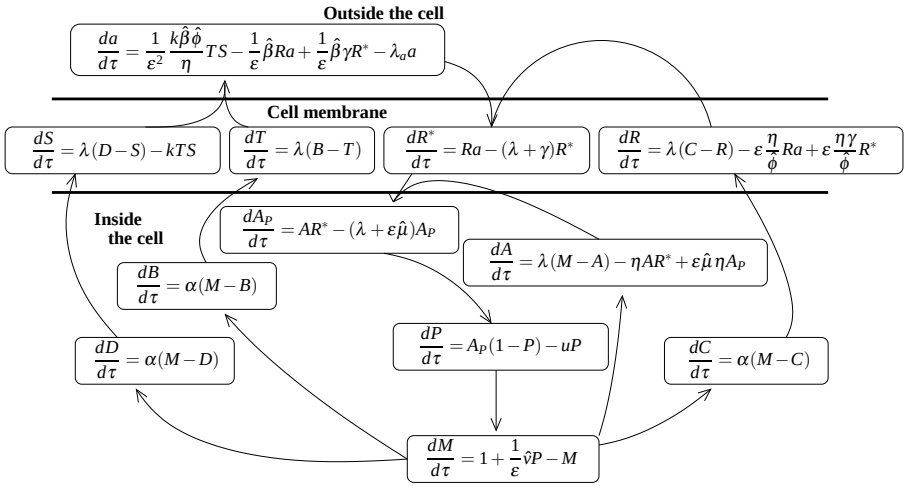

Fig. 5 A schematic representation of the nondimensional model of the *agr* circuit. The parameters are scaled according to (9) and (10), and as discussed at the end of §2.3 we have set $\alpha'_{X,Y} = \alpha$ for $(X,Y) = (B,T),(C,R)$ and (D,S).

and

$$\begin{aligned} \lambda_a' &= \frac{\lambda_a}{\delta_M},\ \nu' = \frac{\nu}{m},\quad \beta' = \frac{\beta\tilde{R}}{\delta_M},\ \eta = \frac{N\delta_M}{b\tilde{A}},\ \gamma' = \frac{\gamma}{\delta_M}, \\ k' &= \frac{k\tilde{T}}{\delta_M},\ u' = \frac{u}{\delta_M},\ \mu' = \frac{\mu}{\delta_M},\ \phi' = \frac{\phi\tilde{S}}{\delta_M}, \end{aligned} \tag{6}$$

where $\tilde{X}$ is the initial condition of X given by (1), for $X = A,T,R,S$.

We assume that protein degradation rates, λ_X in (4), are negligible relative to r so, and since $\delta_X = \lambda_X + r$, we set all the parameters in (4) to be equal. Thus we take

$$\lambda_X' = \lambda \quad \text{for} \quad X = A,T,R,S,R^*,A_P. \tag{7}$$

Dropping $'$'s we get the nondimensional model represented by Figure 5. The dimensionless initial conditions are simply

$$\begin{aligned} M(0) = A(0) = B(0) = C(0) = D(0) = S(0) = T(0) = R(0) = 1, \\ a(0) = R^*(0) = A_P(0) = P(0) = 0. \end{aligned} \tag{8}$$

2.3 Parameter sizes

While the appropriate data required to determine many of the parameter values are not yet available, we do have information about how fast certain reactions take place in relation to others, and this suffices for the qualitative investigations and asymptotic studies on which we focus. The parameter values adopted are consistent in magnitude with the estimates in [11] and this will be discussed further at the end of this section.

Our nondimensionalisations result in the rate of basal mRNA transcription being $O(1)$:

$$\frac{dM}{d\tau} = 1 + \nu' P - M.$$

This basal production exists in order for the QS system to initiate its own activation. The QS-induced rate of transcription must be far greater in order for QS to exhibit switch-like behaviour, with a population of cells becoming rapidly up-regulated. Similarly, we expect the rate at which AIPs bind to the receptors and the rate of AgrA phosphorylation by AgrC to be fast, as we anticipate that reactions involved in signal transduction will be fast compared to processes such as basal transcription and degradation or translation of proteins. For these reasons we define

$$\varepsilon \equiv \frac{m}{\nu},$$

this being the ratio of basal mRNA transcription to QS-induced transcription (this definition is consistent with many other previously published models of QS, see for example [1,6] or [7] where QS-induced production rates are all taken to be considerably greater than the corresponding basal rates; indeed, the choice $\varepsilon << 1$ can be viewed as a mathematical representation of the QS concept), and scale

$$\nu' = \frac{1}{\varepsilon}\hat{\nu}, \quad \beta' = \frac{1}{\varepsilon}\hat{\beta}, \quad \phi' = \frac{1}{\varepsilon}\hat{\phi}, \tag{9}$$

with $\varepsilon << 1$ being our small parameter and hatted parameters being $O(1)$. Choosing these parameters to be of the same order with respect to ε enables the appropriate signal transduction reactions to occur on the same (early) timescales, as would be anticipated biologically. Notice that this will make the rate of AIP production $O(1/\varepsilon^2)$, with

$$\frac{da}{d\tau} = \frac{1}{\varepsilon^2}\frac{k\hat{\beta}\hat{\phi}}{\eta} TS - \frac{1}{\varepsilon}\hat{\beta} Ra + \frac{1}{\varepsilon}\hat{\beta}\gamma R^* - \lambda_a a.$$

This will ensure that at all times and regardless of how active the cells are initially, enough AIP will be produced to upregulate the cells if it is retained within their environment. Notice that the scaling of this production term differs considerably in the equation for $S(t)$; the implication of this is that AgrD is rapidly turned over in the production of AIPs, reflecting the efficiency of the signalling system.

Since we are interested in seeing how the cells become up-regulated, we have the AIP loss rate, λ_a, as $O(1)$, i.e. much smaller than the AIP production rate. However, if we wanted to model a situation where the cells did not become active, say because AIP degradation was too high or the cells were in an open environment where the AIP was lost too quickly into the external environment, then we would alter the parameter choice to account for this by making λ_a much larger than $O(1)$; we will discuss this further in §3.

Taking all other rates of degradation, uptake into the membrane, complex separation and DNA binding to be $O(1)$, we choose only one of the nondimensional parameters to be $O(\varepsilon)$, i.e. smaller than the nondimensional basal transcription, namely

$$\mu' = \varepsilon\hat{\mu}, \tag{10}$$

the rate of housekeeping dephosphorylation of AgrA. Thus we assume that the bacteria can eliminate unwanted phosphorylated AgrA via degradation and dilution sufficiently efficiently to make little of this housekeeping process required (in fact we will see that it does not affect the leading-order behaviour of the system on any timescale). For an asymptotic analysis of an alternative parameter set see [15], where we, in addition, chose $k = O(\varepsilon)$, i.e. AgrD loss as a result of AIP production was assumed to be relatively slow. However, the choice for this paper ($k = O(1)$) results in two fewer timescales with no significant changes to our conclusions.

Thus our overall parameter choice is motivated by a desire to ensure that the mathematical analysis be revealing as well as biologically plausible. For example, choosing β' and ϕ' to be $O(1/\varepsilon)$ implies that the TCS reactions occur on the timescale on which AIPs are first produced in significant numbers, so that the signal transduction process begins immediately (as is desirable), with these signal transduction reactions and AIP production being the only reactions that occur at leading order here, thus enabling us to examine them effectively in isolation. Numerical investigations (not shown) indicate that the rapid switch-like upregulation which we know occurs *in vitro* (see for example, [17]) is dependent upon this parameter choice. For instance, sufficiently small values of ν' (even in the case where $\lambda_a = 0$) result in the cells remaining in a down-regulated state (this will be addressed further at the end of the asymptotic analysis), while reducing β' and ϕ' slows down the switch between the inactive and active states.

As mentioned earlier, our parameter choice follows a similar line to that used for simulations in [11] by Gustafsson *et al.*, wherein reactions involved in the activation of the TCS were assumed to take place faster than, say, basal transcription and degradation, their choice being based as far as possible upon their experimental evidence. The two models differ in a number of ways: specifically, [11] considers the influence of SarA on transcription of the operon and takes the AIP concentration to be a parameter of the model, rather than a variable (as discussed earlier); saturation kinetics are described explicitly in [11], while we use the equation representing P, the proportion of up-regulated cells, to incorporate this implicitly. Hence there is a certain amount of overlap between the two parameter sets but each model also requires distinct additional parameters. Of those in [11] which are equivalent to ours, activation rates are five times the size of degradation rates, one hundred times the size of the spontaneous separation (between AIP and receptors) rates and ten times all the remaining parameters (in ours they are $O(1/\varepsilon)$ larger), so that the nondimensional parameters directly involved in activation of the QS system are assumed to be the largest parameters in both our model and in [11].

Unless otherwise stated, all dimensionless parameters in our numerical solutions (except ε) will be taken to be unity, with $\varepsilon = 10^{-3}$. For simplicity we henceforth write $\alpha'_{X,Y} = \alpha$ for $(X,Y) = (B,T),(C,R)$ and (D,S) (which is equivalent to assuming that AgrB and AgrC are taken into the membrane at equal rates and that AgrD is anchored at this same rate) and drop all primes. The associated default values of the unhatted dimensionless parameters are displayed in Table 3 (all hatted quantities are unity).

Table 3 The default parameter set.

Nondimensional parameter	Default value
μ	10^{-3}
$\alpha, \lambda, \lambda_a, \eta, \gamma, k, u$	1
ν, β, ϕ	10^3
ε	10^{-3}

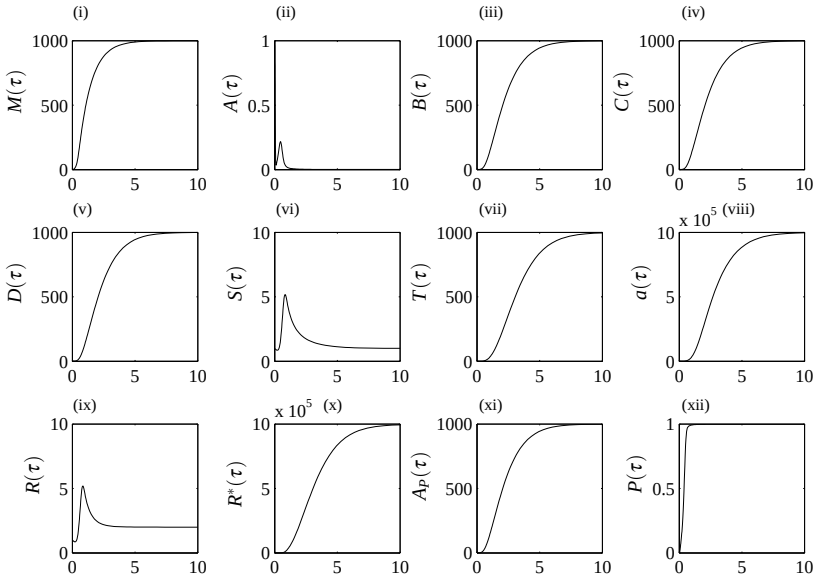

Fig. 6 Numerical solutions to the nondimensional model using the initial conditions (8) and parameter scalings given by (9)-(10) with the default parameter set in Table 3. The shift from an inactive to an active state, reflecting the increased AIP levels in (viii), is evident as P approaches unity in (xii).

3 Numerical simulation

Figure 6 illustrates a numerical solution to the nondimensional model using the initial conditions (8) and the default parameter set given in Table 3. From (viii) and (x) (or see Figure 8 for a clearer picture of the initial behaviour) we see that AIP production begins immediately and the AIPs then bind to any available receptors, resulting in a loss of free transmembrane AgrC, illustrated in (ix). The bound receptors phosphorylate AgrA within the cell, leading to increased levels of activated AgrA, (xi), and a corresponding rapid decrease in the amount of inactive AgrA, (ii). This is enough to kick-start the QS-controlled mRNA transcription (transcription initially being only at the basal level) - see the increase in (i) - and this forces a small increase in the level both of inactive AgrA, (ii), and of free receptors, (ix). Due to increased mRNA levels, we also see increased levels of all the other proteins, represented in (iii)-(vii) (although the increase in transmembrane AgrD in (vi) is short-lived as it is turned over in the production of AIP), which enable the continued production of AIPs, pro-

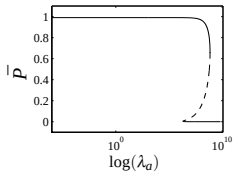

Fig. 7 The steady-state solution for P against $\log(\lambda_a)$ (calculated in XPPAUT 5.91), illustrating the three regimes (solid lines represent stable steady states, with dashed lines being unstable). Here we have used $\varepsilon = 10^{-2}$. The system is bistable within an intermediate range of λ_a, meaning that the population can switch quickly (but hysteretically) between down- and up-regulated states (for sufficiently small λ_a the system will always reach an up-regulated state and for sufficiently large λ_a the *agr* operon will be unable to activate itself). Our default choice for λ_a is $\lambda_a = 1$.

ducing a clear transition to an up-regulated state, with P becoming close to unity, see (xii). In consequence, the increase in A and R only lasts a short while and is quickly replaced by a sharp drop in their concentration levels as they are consumed in the activation process. We will see in the asymptotic analysis that the drop in A occurs on the same timescale as that for the cells to reach an up-regulated state (those of R and S occur on a longer timescale).

This numerical solution demonstrates how a large population of *S. aureus* would, after a time lag, shift from a down-regulated, and relatively harmless, state to a highly virulent one if sufficient AIP is retained in the environment of the cells. For comparison, in Figure 7 we have displayed the solution curve of P, the proportion of *agr*-active cells, for varying λ_a, the AIP degradation rate (this can also be interpreted as the rate at which AIP is lost in the external environment). We see that the model displays the bi-stable behaviour which is often viewed as typical of QS systems, see [6] or [7] for example, enabling the QS system to switch rapidly between down- and up-regulated states depending on the environment of the cells. In [15] we demonstrate that an alternative way to ensure that the cells either do not reach an active state, or at least that the time at which this occurs is delayed, is through inhibition of the *agr* operon via competitive binding at the receptor sites, as discussed in §1.3.

4 Asymptotic analysis for $\varepsilon \to 0$

We now perform a time-dependent asymptotic analysis on the model in order to clarify its behaviour, the full model being too involved to allow a great deal of insight. Moreover, it is valuable when adding extra processes to the system (while keeping its complexity under control) to have in place systematically-derived sub-models of the type we obtain below. For an overview of asymptotic methods see [18], for example.

We first note that, since their initial conditions are equal and we have assumed their depletion rates are also equal, we have

$$B(\tau) \equiv C(\tau) \equiv D(\tau) \tag{11}$$

for all τ, so henceforth we eliminate C and D in favour of B.

The asymptotic structure is complicated, there being eight timescales in all, the first to arise reading $\hat{\tau} = \tau/\varepsilon$. Initially only the fastest reactions feature, namely those

involved in signal transduction, for example AIP binding, with the slower reactions, such as dilution, contributing on the longer timescales. The scalings required for all the variables on each timescale are given in Table 4. In each case the scalings are given relative to the dimensionless variables defined in (2) and (3). On each timescale we manipulate the long-term or near-blow-up behaviour of the system to determine the appropriate scalings for the following timescale. For instance, if the long-term behaviour of a particular variable X is $X \sim \tau$ as $\tau \to \infty$, then X will be scaled in the same way as τ to move to the subsequent timescale. Each timescale brings new reactions into the leading-order behaviour. Mathematically, these can only occur in a specific sequence and it is this which dictates the scalings for τ on each timescale. Additionally, on each timescale the small-time behaviour must match the long-time behaviour on the preceding timescale.

In the interests of brevity, we do not provide details of all the timescales; instead we choose those which demonstrate the most interesting aspects of the system, namely those describing signal transduction, the cells becoming *agr* active and their approach to steady state. We believe that the timescales described in detail in the main text are both biologically and mathematically interesting, providing insight into the dynamics of the *agr* system, while illustrating the techniques used in such an asymptotic analysis. The remaining timescales are described briefly in the Appendix (and, for clarity, Table 4 contains the scalings for all timescales). In all comparisons between the numerical solutions and the asymptotic approximations we use $\varepsilon = 10^{-3}$ and variables are always plotted against τ in its unscaled form. The numerical solutions to the full model are represented by solid lines, while the asymptotic approximations are given by dashed ones.

4.1 Initial timescale: signal production and the two-component system

We find that on the first four timescales

$$B = R = S = T = 1 \tag{12}$$

hold to leading order in ε because translation occurs at a negligible rate in comparison with the TCS reactions and transcription, which already come into balance during the early stages of the QS process. This gives the simplified system

$$\frac{dM}{d\tau} = \frac{1}{\varepsilon}\hat{\nu}P - M + 1, \tag{13}$$

$$\frac{dA}{d\tau} = \lambda(M - A) - \eta A R^* + \varepsilon\hat{\mu}\eta A_P, \tag{14}$$

$$\frac{da}{d\tau} = \frac{1}{\varepsilon^2}\frac{k\hat{\beta}\hat{\phi}}{\eta} - \frac{1}{\varepsilon}\hat{\beta}a + \frac{1}{\varepsilon}\hat{\beta}\gamma R^* - \lambda_a a, \tag{15}$$

$$\frac{dR^*}{d\tau} = a - (\lambda + \gamma)R^*, \tag{16}$$

$$\frac{dA_P}{d\tau} = AR^* - (\lambda + \varepsilon\hat{\mu})A_P, \tag{17}$$

$$\frac{dP}{d\tau} = A_P(1 - P) - uP. \tag{18}$$

Equations (14)-(17) could be viewed in their own right as a generic model of a positive feedback loop containing a TCS in which a plentiful supply of receptors is

Table 4 Summary of the scalings required for the asymptotic approximations for the variables on each of the timescales. A variable is left blank on a specific timescale if it does not require rescaling on that timescale. The scalings by themselves provide some insight into which variables dominate the behaviour at each stage; for example, the AIP concentration is large on the early timescales because it acts as the catalyst of the QS-related signal transduction. We have introduced the time shifts $\tau_3 \sim ((\ln(1/\varepsilon) - \ln\ln(1/\varepsilon))/k\hat{\phi})^{\frac{1}{2}}$ and $\tau_6 \sim \varepsilon^{-\frac{1}{6}}(\eta/\lambda\hat{v})^{\frac{1}{3}}\ln(1/\varepsilon)/3 + \tau_3$. Notice from these time shifts that we will see two time lags, the second being larger. A derivation of τ_3 (in particular why the $\ln\ln(1/\varepsilon)$ term is required) is provided in §4.3.

	VARIABLE										
TIMESCALE	τ	M	A	B	S	T	a	R	R^*	A_P	P
1	$\varepsilon\hat{\tau}$	-	-	-	-	-	$\varepsilon^{-1}\hat{a}$	-	-	$\varepsilon\hat{A}_P$	$\varepsilon^2\hat{p}$
2	$\varepsilon^{\frac{1}{2}}\tau^\dagger$	-	-	-	-	-	$\varepsilon^{-1}a^\dagger$	-	$\varepsilon^{-\frac{1}{2}}R^{*\dagger}$	-	$\varepsilon^{\frac{1}{2}}P^\dagger$
3	$\varepsilon^{\frac{1}{2}}\tau_3 + \varepsilon^{\frac{1}{2}}\ln^{-\frac{1}{2}}(1/\varepsilon)\tau^\ddagger$	$\ln(1/\varepsilon)M^\ddagger$	$\varepsilon^{\frac{1}{2}}\ln^{\frac{1}{2}}(1/\varepsilon)A^\ddagger$	-	-	-	$\varepsilon^{-1}a^\ddagger$	-	$\varepsilon^{-\frac{1}{2}}\ln^{\frac{1}{2}}(1/\varepsilon)R^{*\ddagger}$	-	$\varepsilon^{\frac{1}{2}}\ln^{\frac{1}{2}}(1/\varepsilon)P^\ddagger$
4	$\varepsilon^{\frac{1}{2}}\tau_3 + \varepsilon^{\frac{1}{2}}\ln^{\frac{1}{2}}(1/\varepsilon)\tau^+$	$\ln(1/\varepsilon)M^+$	$\varepsilon^{\frac{1}{2}}\ln^{\frac{1}{2}}(1/\varepsilon)A^+$	-	-	-	$\varepsilon^{-1}a^+$	-	$\varepsilon^{-\frac{1}{2}}\ln^{\frac{1}{2}}(1/\varepsilon)R^{*+}$	-	$\varepsilon^{\frac{1}{2}}\ln^{\frac{1}{2}}(1/\varepsilon)P^+$
5	$\varepsilon^{\frac{1}{2}}\tau_3 + \varepsilon^{\frac{1}{3}}\check{\tau}$	$\varepsilon^{-\frac{1}{3}}\check{M}$	$\varepsilon^{\frac{1}{3}}\check{A}$	-	-	-	$\varepsilon^{-1}\check{a}$	-	$\varepsilon^{-\frac{2}{3}}\check{R}^*$	-	$\varepsilon^{\frac{1}{3}}\check{P}$
6	$\varepsilon^{\frac{1}{2}}\tau_6 + \varepsilon^{\frac{1}{3}}\check{\tau}$	$\varepsilon^{-\frac{2}{3}}\check{M}$	$\ln^{-1}(1/\varepsilon)\check{A}$	$\varepsilon^{-\frac{1}{3}}\check{B}$	-	-	$\varepsilon^{-1}\check{a}$	-	$\varepsilon^{-\frac{2}{3}}\ln(1/\varepsilon)\check{R}^*$	$\varepsilon^{-\frac{1}{3}}\check{A}_P$	-
7	$\varepsilon^{\frac{1}{2}}\tau_6 + \varepsilon^{\frac{1}{4}}\tau'$	$\varepsilon^{-\frac{3}{4}}M'$	$\varepsilon^{\frac{1}{2}}A'$	$\varepsilon^{-\frac{1}{2}}B'$	$\varepsilon^{-\frac{1}{4}}S'$	$\varepsilon^{-\frac{1}{4}}T'$	$\varepsilon^{-\frac{5}{4}}a'$	$\varepsilon^{-\frac{1}{4}}R'$	$\varepsilon^{-\frac{5}{4}}R^{*\prime}$	$\varepsilon^{-\frac{1}{2}}A_P{}'$	-
8	$\varepsilon^{\frac{1}{2}}\tau_6 + \bar{\tau}$	$\varepsilon^{-1}\bar{M}$	$\varepsilon\bar{A}$	$\varepsilon^{-1}\bar{B}$	-	$\varepsilon^{-1}\bar{T}$	$\varepsilon^{-2}\bar{a}$	-	$\varepsilon^{-2}\bar{R}^*$	$\varepsilon^{-1}\bar{A}_P$	-

available, and where the feedback affects the response regulator alone (as would be relevant to many loops of this kind in other bacteria), thus making their asymptotic analysis open to more general application. As mentioned previously, the additional upregulation feeding into the signal precursors and receptors of the *agr* operon makes it a more involved feedback loop than most and this will be discussed further in §5.

The above equations involve the signal molecule (a), bound receptor (R^*), monitoring the signal level, the response regulator (in both its active and inactive forms, A_P and A respectively), the proportion of active cells (P) and, finally, mRNA (M) whose production rate is dependent upon P and which determines the production rate of the response regulator, thus completing the feedback loop. The rescaled equations on the first timescale (see Table 4) become

$$\frac{dM}{d\hat{\tau}} = \varepsilon^2\hat{\nu}\hat{P} - \varepsilon M + \varepsilon, \tag{19}$$

$$\frac{dA}{d\hat{\tau}} = \varepsilon\lambda(M-A) - \varepsilon\eta A R^* + \varepsilon^3\hat{\mu}\eta\hat{A}_P, \tag{20}$$

$$\frac{d\hat{a}}{d\hat{\tau}} = \frac{k\hat{\beta}\hat{\phi}}{\eta} - \hat{\beta}\hat{a} + \varepsilon\hat{\beta}\gamma R^* - \varepsilon\lambda_a\hat{a}, \tag{21}$$

$$\frac{d\hat{A}_P}{d\hat{\tau}} = AR^* - \varepsilon(\lambda+\varepsilon\hat{\mu})\hat{A}_P, \tag{22}$$

$$\frac{dR^*}{d\hat{\tau}} = \hat{a} - \varepsilon(\lambda+\gamma)R^*, \tag{23}$$

$$\frac{d\hat{P}}{d\hat{\tau}} = \hat{A}_P(1-\varepsilon^2\hat{P}) - \varepsilon u\hat{P}, \tag{24}$$

so disregarding the $O(\varepsilon)$ or smaller terms gives a linear leading-order system which can be solved sequentially (in the order shown), to give

$$M(\hat{\tau}) = A(\hat{\tau}) = 1, \quad \hat{a}(\hat{\tau}) = \frac{k\hat{\phi}}{\eta}(1-e^{-\hat{\beta}\hat{\tau}}), \quad R^*(\hat{\tau}) = \frac{k\hat{\phi}}{\eta}\hat{\tau} - \frac{k\hat{\phi}}{\hat{\beta}\eta}(1-e^{-\hat{\beta}\hat{\tau}}),$$

$$\hat{A}_P(\hat{\tau}) = \frac{k\hat{\phi}}{2\eta}\hat{\tau}^2 - \frac{k\hat{\phi}}{\hat{\beta}\eta}\hat{\tau} + \frac{k\hat{\phi}}{\hat{\beta}^2\eta}(1-e^{-\hat{\beta}\hat{\tau}}),$$

$$\hat{P}(\hat{\tau}) = \frac{k\hat{\phi}}{6\eta}\hat{\tau}^3 - \frac{k\hat{\phi}}{2\hat{\beta}\eta}\hat{\tau}^2 + \frac{k\hat{\phi}}{\hat{\beta}^2\eta}\hat{\tau} - \frac{k\hat{\phi}}{\hat{\beta}^3\eta}(1-e^{-\hat{\beta}\hat{\tau}}).$$

The increasing sequence of powers of $\hat{\tau}$ (with the exception of $\hat{a}$) is associated with each of the relevant quantities being downstream of the previous one (see Figure 1).

We see from Figure 8 that these approximations are accurate in the initial stages. As we had anticipated, it is the TCS reactions which occur first. Note that k represents the rate of AIP production, $\hat{\phi}$ the rate of AgrA phosphorylation, $\hat{\beta}$ the rate of AgrC-AIP binding and $1/\eta$ the rate at which AgrA binds to DNA. At this stage these four parameters control the behaviour of the system: AIP is rapidly produced and binds to the free receptors, resulting in the commencement of the phosphorylation cascade; this gives an increased level of activator, A_P, in the cells. $R^*(\hat{\tau})$, $\hat{A}_P(\hat{\tau})$ and $\hat{P}(\hat{\tau})$ display unbounded growth as $\hat{\tau}\to+\infty$ because all the reactions involved in their leading-order behaviour are 'production' terms: we see increased levels of R^* due to AIP binding to receptors, which activate AgrA to form $\hat{A}_P$, and $\hat{P}$ in turn increases as a direct result of this AgrA activation. The unbounded growth is associated with the absence of reactions that involve sink terms for these quantities, for example the loss

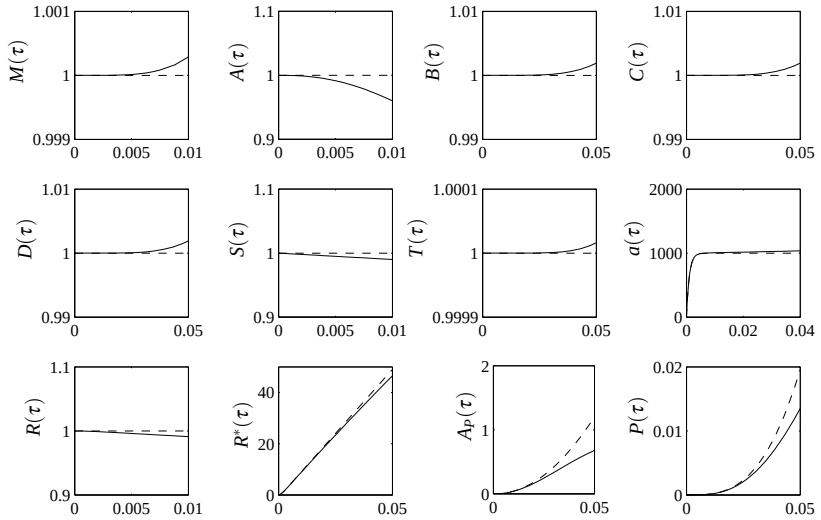

Fig. 8 A comparison of the asymptotic and numerical solutions on the initial timescale. The solutions of the full model are represented by the full lines and the asymptotic approximations on the initial timescale by the dashed lines. Notice that, in order to be able to see where the asymptotic approximations begin to fail in each case, certain variables are plotted over a longer timescale than others. $\hat{\tau} = 1$ corresponds to $\tau = 10^{-3}$. We recall that the variables are plotted against τ in its unscaled form; the same applies in all the figures which follow.

of AgrA through its activation which, as we now show, enters on the next timescale (dilution is negligible until the final timescale).

4.2 Second timescale: transcription

The next stage is for significant mRNA transcription to begin. The rescaled equations are

$$\frac{dM}{d\tau^\dagger} = \hat{\nu}P^\dagger - \varepsilon^{\frac{1}{2}}M + \varepsilon^{\frac{1}{2}}, \tag{25}$$

$$\frac{dA}{d\tau^\dagger} = \varepsilon^{\frac{1}{2}}\lambda(M-A) - \eta AR^{*\dagger} + \varepsilon^{\frac{3}{2}}\hat{\mu}\eta A_P, \tag{26}$$

$$\varepsilon^{\frac{1}{2}}\frac{da^\dagger}{d\tau^\dagger} = \frac{k\hat{\beta}\hat{\phi}}{\eta} - \hat{\beta}a^\dagger + \varepsilon^{\frac{1}{2}}\hat{\beta}\gamma R^{*\dagger} - \varepsilon\lambda_a a^\dagger, \tag{27}$$

$$\frac{dR^{*\dagger}}{d\tau^\dagger} = a^\dagger - \varepsilon^{\frac{1}{2}}(\lambda+\gamma)R^{*\dagger}, \tag{28}$$

$$\frac{dA_P}{d\tau^\dagger} = AR^{*\dagger} - \varepsilon^{\frac{1}{2}}(\lambda+\varepsilon\hat{\mu})A_P, \tag{29}$$

$$\frac{dP^\dagger}{d\tau^\dagger} = A_P(1-\varepsilon^{\frac{1}{2}}P^\dagger) - \varepsilon^{\frac{1}{2}}uP^\dagger. \tag{30}$$

Taking the leading-order terms of (25)-(30) gives a linear system which can again be solved sequentially and, matching to the previous timescale, we have

$$\begin{aligned} a^\dagger(\tau^\dagger) &= \frac{k\hat{\phi}}{\eta}, \quad R^{*\dagger}(\tau^\dagger) = \frac{k\hat{\phi}}{\eta}\tau^\dagger, \quad A(\tau^\dagger) = e^{-\frac{k\hat{\phi}}{2}\tau^{\dagger 2}}, \\ A_P(\tau^\dagger) &= \frac{1}{\eta}(1-e^{-\frac{k\hat{\phi}}{2}\tau^{\dagger 2}}), \end{aligned} \tag{31}$$

together with

$$P^\dagger(\tau^\dagger) = \frac{1}{\eta}\left(\tau^\dagger - \frac{1}{2}\sqrt{\frac{2\pi}{k\hat{\phi}}}\,\mathrm{erf}\left(\frac{1}{2}\sqrt{2k\hat{\phi}}\,\tau^\dagger\right)\right),$$

$$M(\tau^\dagger) = \frac{\hat{\nu}}{\eta}\left(\frac{\tau^{\dagger 2}}{2} - \frac{1}{2}\sqrt{\frac{2\pi}{k\hat{\phi}}}\,\tau^\dagger\,\mathrm{erf}\left(\frac{1}{2}\sqrt{2k\hat{\phi}}\,\tau^\dagger\right) - \frac{1}{k\hat{\phi}}e^{-\frac{k\hat{\phi}}{2}\tau^{\dagger 2}} + \frac{1}{k\hat{\phi}} + \frac{\eta}{\hat{\nu}}\right),$$

so that

$$P^\dagger(\tau^\dagger) \sim \frac{1}{\eta}\tau^\dagger, \quad M(\tau^\dagger) \sim \frac{\hat{\nu}}{2\eta}\tau^{\dagger 2} \quad \text{as} \quad \tau^\dagger \to +\infty.$$

Thus on this timescale, like the previous and many of the subsequent ones (indeed only timescales 6 and 7 are not susceptible to exact leading-order solutions), simple explicit leading-order solutions are available, despite the complexity of the full system. This is in striking contrast to the full system of equations which can be solved only numerically.

The (fast) TCS reaction is in quasi-equilibrium here (i.e. $a^\dagger \sim k\hat{\phi}TS/\eta R$) and will remain so until the final timescale. On this second timescale, the free AIP concentration thus levels off as a balance is attained between its production and its loss due to binding to the receptors but, importantly, the levels of non-phosphorylated AgrA become exponentially small (see (31)) as more and more AgrA is activated via the TCS, while, to leading order, no more is being translated to replace this loss (as mentioned in §3). We again see unbounded growth of $R^{*\dagger}$, $P^\dagger$ and now also M, as *agr* mRNA is transcribed at leading order, while the A_P level saturates due to the exponential decrease of A (so that little further A_P can be generated by its activation). Figure 9 illustrates those variables whose approximations differ from those on the initial timescale.

4.3 Third timescale: AgrA translation

With the approximation (31), $A(\tau^\dagger)$ degrades to zero due to the absence at leading order of AgrA translation - the scalings for this third timescale bring the latter into prominence. We now provide the justification for the somewhat-subtle τ scaling noted in Table 4 (the remaining scalings therein follow as a direct result of the τ scaling).

In order to bring the AgrA translation term, i.e. λM, into the leading-order behaviour of (26), we need to choose our scalings such that

$$\frac{\varepsilon^{\frac{1}{2}}M}{AR^{*\dagger}} = O(1). \tag{32}$$

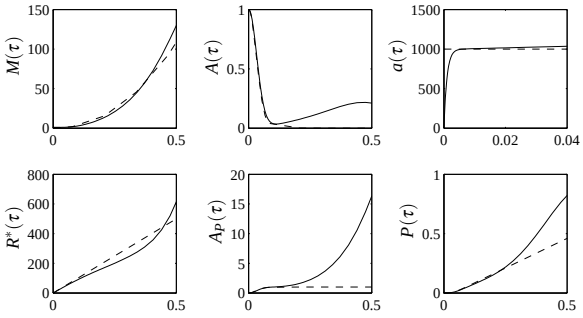

Fig. 9 A comparison of the asymptotic and numerical solutions on the second timescale. In contrast to the first timescale we now see the transcription of mRNA and the decrease in the level of inactive AgrA which occurs as a result of its phosphorylation. We also now attain a constant level of AIP following its initial production, the AIP remaining close to this level until AgrB and AgrD become transmembrane in significant amounts on timescale 6. $\tau^\dagger = 1$ corresponds to $\tau \approx 0.0316$.

However, we know that (roughly speaking) the matching conditions

$$M \sim \tau^{\dagger 2}, \quad A \sim e^{-\frac{k\hat{\phi}}{2}\tau^{\dagger 2}}, \quad R^{*\dagger} \sim \tau^\dagger \quad \text{as} \quad \tau^\dagger \to +\infty,$$

pertain from the previous timescale, so that (32) is equivalent to

$$\varepsilon^{\frac{1}{2}}\tau^\dagger \sim e^{-\frac{k\hat{\phi}}{2}\tau^{\dagger 2}}.$$

This balance implies the rather delicate scalings that appear in Table 4: our choice of $\tau^\ddagger$ implies that $\varepsilon^{\frac{1}{2}}\tau^\dagger$ and $e^{-\frac{k\hat{\phi}}{2}\tau^{\dagger 2}}$ are each of $O(\varepsilon^{\frac{1}{2}}\ln^{\frac{1}{2}}(1/\varepsilon))$ for $\tau^\ddagger = O(1)$, so that (32) does indeed hold. With all the new scalings, equations (25)-(30) become

$$\frac{dM^\ddagger}{d\tau^\ddagger} = \ln^{-1}(1/\varepsilon)\hat{\nu}P^\ddagger - \varepsilon^{\frac{1}{2}}\ln^{-\frac{1}{2}}(1/\varepsilon)M^\ddagger + \varepsilon^{\frac{1}{2}}\ln^{-\frac{3}{2}}(1/\varepsilon), \tag{33}$$

$$\frac{dA^\ddagger}{d\tau^\ddagger} = \lambda M^\ddagger - \varepsilon^{\frac{1}{2}}\ln^{-\frac{1}{2}}(1/\varepsilon)\lambda A^\ddagger - \eta A^\ddagger R^{*\ddagger} + \varepsilon\ln^{-1}(1/\varepsilon)\hat{\mu}\eta A_P, \tag{34}$$

$$\varepsilon^{\frac{1}{2}}\ln^{\frac{1}{2}}(1/\varepsilon)\frac{da^\ddagger}{d\tau^\ddagger} = \frac{k\hat{\beta}\hat{\phi}}{\eta} - \hat{\beta}a^\ddagger + \varepsilon^{\frac{1}{2}}\ln^{\frac{1}{2}}(1/\varepsilon)\hat{\beta}\gamma R^{*\ddagger} - \varepsilon\lambda_a a^\ddagger, \tag{35}$$

$$\frac{dR^{*\ddagger}}{d\tau^\ddagger} = \ln^{-1}(1/\varepsilon)a^\ddagger - \varepsilon^{\frac{1}{2}}\ln^{-\frac{1}{2}}(1/\varepsilon)(\lambda+\gamma)R^{*\ddagger}, \tag{36}$$

$$\frac{dA_P}{d\tau^\ddagger} = \varepsilon^{\frac{1}{2}}\ln^{\frac{1}{2}}(1/\varepsilon)A^\ddagger R^{*\ddagger} - \varepsilon^{\frac{1}{2}}\ln^{-\frac{1}{2}}(1/\varepsilon)(\lambda+\varepsilon\hat{\mu})A_P, \tag{37}$$

$$\frac{dP^\ddagger}{d\tau^\ddagger} = \ln^{-1}(1/\varepsilon)A_P - \varepsilon^{\frac{1}{2}}\ln^{-\frac{1}{2}}(1/\varepsilon)A_P P^\ddagger - \varepsilon^{\frac{1}{2}}\ln^{-\frac{1}{2}}(1/\varepsilon)uP^\ddagger. \tag{38}$$

Hence we see that, on this short transition timescale, all the variables maintain a constant level at leading order in $1/\ln(1/\varepsilon)$, except for $A^\ddagger$ which now decays exponentially to a strictly positive constant (rather than to zero), i.e. we have (on matching

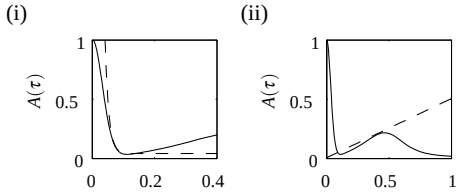

Fig. 10 On the second timescale, AgrA is lost primarily due to its phosphorylation. Here we illustrate the asymptotic approximation on the (i) third and (ii) fourth timescales, showing how its level builds back up somewhat. The limit behaviour of A as $\tau^{\ddagger} \to \infty$ (on the third timescale) represents the first turning point of $A(\tau)$. $\tau^{\ddagger} = 1$ corresponds to $\tau \approx 0.0826$. On the fourth timescale we see clearly the increase in AgrA concentration as a result of its translation (details are given in the Appendix). This increase continues until the population becomes up-regulated, at which point the activation of AgrA dominates its translation. $\tau^{+} = 1$ corresponds to $\tau \approx 0.1536$.

to the previous timescale) the leading-order solutions (the correction terms being only logarithmically smaller in ε):

$$M^{\ddagger} = \frac{\hat{\nu}}{2\eta k\hat{\phi}}, \quad a^{\ddagger} = \frac{k\hat{\phi}}{\eta}, \quad R^{*\ddagger} = \frac{1}{\eta}\sqrt{k\hat{\phi}}, \quad A_P = \frac{1}{\eta}, \quad P^{\ddagger} = \frac{1}{\eta}\sqrt{\frac{1}{k\hat{\phi}}},$$

and, finally and most importantly here,

$$A^{\ddagger} = A_c^{\ddagger} + e^{-\sqrt{k\hat{\phi}}\tau^{\ddagger}}, \quad A_c^{\ddagger} \equiv \frac{\lambda\hat{\nu}\sqrt{k\hat{\phi}}}{2\eta k^2\hat{\phi}^2}.$$

Figure 10(i) demonstrates that $A_c^{\ddagger}$ relates to the first turning point in $A(\tau)$, at which the initial decrease in AgrA concentration turns around fairly rapidly to produce a small rise associated with its translation becoming evident at leading order[2]. Physically this constant is dictated by the balance between AgrA translation and its activation. The subsequent rise in AgrA occurs on the fourth timescale, some details of which can be found (together with those of the fifth and seventh) in the Appendix, with a plot given in Figure 10(ii).

4.4 Sixth timescale: proteins move into the cell membrane causing the feedback loop to be fully established

We now skip to the sixth timescale, where following AgrA translation on the fourth timescale and AgrB, C and D translation on the fifth (see the Appendix), we expect a proportion of AgrB and AgrC to enter the cell membrane and AgrD to become

[2] $A_c^{\ddagger}$, for the default parameter values, corresponds to $A_c = \varepsilon^{\frac{1}{2}} \ln^{\frac{1}{2}}(1/\varepsilon) A_c^{\ddagger} = 0.0416$.

anchored to the membrane ((12) no longer applies). The rescaled equations are

$$\frac{d\check{M}}{d\check{\tau}} = \hat{v}P - \varepsilon^{\frac{1}{3}}\check{M} + \varepsilon, \tag{39}$$

$$\varepsilon^{\frac{1}{3}}\ln^{-1}(1/\varepsilon)\frac{d\check{A}}{d\check{\tau}} = \lambda\check{M} - \varepsilon^{\frac{2}{3}}\ln^{-1}(1/\varepsilon)\lambda\check{A} - \eta\check{A}\check{R}^* + \varepsilon^{\frac{4}{3}}\hat{\mu}\eta\check{A}_P, \tag{40}$$

$$\frac{d\check{B}}{d\check{\tau}} = \alpha\check{M} - \varepsilon^{\frac{1}{3}}\alpha\check{B}, \tag{41}$$

$$\frac{dS}{d\check{\tau}} = \lambda\check{B} - \varepsilon^{\frac{1}{3}}\lambda S - \varepsilon^{\frac{1}{3}}kTS, \tag{42}$$

$$\frac{dT}{d\check{\tau}} = \lambda\check{B} - \varepsilon^{\frac{1}{3}}\lambda T, \tag{43}$$

$$\varepsilon^{\frac{2}{3}}\frac{d\check{a}}{d\check{\tau}} = \frac{k\hat{\beta}\hat{\phi}}{\eta}TS - \hat{\beta}R\check{a} + \varepsilon^{\frac{1}{3}}\ln(1/\varepsilon)\hat{\beta}\gamma\check{R}^* - \varepsilon\lambda_a\check{a}, \tag{44}$$

$$\frac{dR}{d\check{\tau}} = \lambda\check{B} - \varepsilon^{\frac{1}{3}}\lambda R - \varepsilon^{\frac{1}{3}}\frac{\eta}{\hat{\phi}}R\check{a} + \varepsilon^{\frac{2}{3}}\ln(1/\varepsilon)\frac{\eta\gamma}{\hat{\phi}}\check{R}^*, \tag{45}$$

$$\frac{d\check{R}^*}{d\check{\tau}} = \ln^{-1}(1/\varepsilon)R\check{a} - \varepsilon^{\frac{1}{3}}(\lambda+\gamma)\check{R}^*, \tag{46}$$

$$\frac{d\check{A}_P}{d\check{\tau}} = \check{A}\check{R}^* - \varepsilon^{\frac{1}{3}}(\lambda + \varepsilon\hat{\mu})\check{A}_P, \tag{47}$$

$$\frac{dP}{d\check{\tau}} = \check{A}_P(1-P) - \varepsilon^{\frac{1}{3}}uP. \tag{48}$$

The leading-order terms give,

$$\check{R}^* = \frac{k\hat{\phi}}{3\eta\omega}, \qquad \check{A}(\check{\tau}) = \frac{\lambda\check{M}}{\eta\check{R}^*}, \qquad \check{a}(\check{\tau}) = \frac{k\hat{\phi}TS}{\eta R},$$

and the nonlinear coupled system

$$\frac{d\check{M}}{d\check{\tau}} = \hat{v}P, \qquad \frac{dP}{d\check{\tau}} = \check{A}_P(1-P), \qquad \frac{d\check{A}_P}{d\check{\tau}} = \frac{\lambda}{\eta}\check{M}. \tag{49}$$

Finally, we also have

$$\frac{d\check{B}}{d\check{\tau}} = \alpha\check{M}, \qquad \frac{dS}{d\check{\tau}} = \frac{dT}{d\check{\tau}} = \frac{dR}{d\check{\tau}} = \lambda\check{B}, \tag{50}$$

which can be solved sequentially once (49) has been (with $\check{B}$ growing in parallel with $\alpha\eta\check{A}_P/\lambda$). Matching to the fifth timescale requires

$$\check{M} \sim \frac{\omega}{3\lambda}e^{\omega\check{\tau}}, \quad \check{P} \sim \frac{1}{3\omega\eta}e^{\omega\check{\tau}}, \quad \check{A}_P \sim \frac{1}{3\eta}e^{\omega\check{\tau}}, \quad \check{B} \sim \frac{\alpha}{3\lambda}e^{\omega\check{\tau}}, \quad S,T,R \sim 1 \tag{51}$$

as $\check{\tau} \to -\infty$, where $\omega = (\lambda\hat{v}/\eta)^{\frac{1}{3}}$. The slower processes which control protein behaviour are now operating alongside quicker signal transduction reactions (which

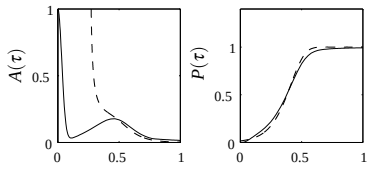

Fig. 11 Asymptotic approximation (dashed line) and numerical solution (solid line) for inactive AgrA and for the proportion of up-regulated cells on the sixth timescale, with the initial conditions for the asymptotic approximation given by (51). P nearing unity as $\check{\tau} \to \infty$ corresponds to (almost) the whole population of cells becoming up-regulated. We see a decrease in AgrA as the loss of this protein via activation again takes dominance over its translation.

have reached quasi-equilibrium - see (40) and (44)). We observe from the numerical solution to (49) that P quickly levels off to unity, see Figure 11, implying that as $\check{\tau} \to +\infty$,

$$\begin{aligned} &P \to 1, && \check{M} \sim \hat{\nu}\check{\tau}, && \check{B} \sim \frac{\alpha\hat{\nu}}{2}\check{\tau}^2, \\ &R,S,T \sim \frac{\alpha\lambda\hat{\nu}}{6}\check{\tau}^3, && \check{a} \sim \frac{k\hat{\phi}\alpha\lambda\hat{\nu}}{6\eta}\check{\tau}^3, && \check{A}_P \sim \frac{\lambda\hat{\nu}}{2\eta}\check{\tau}^2. \end{aligned} \tag{52}$$

Expanding R^* in (46) in terms of $1/\ln(1/\varepsilon)$ we see that

$$\frac{d\check{R}^*}{d\check{\tau}} \sim \frac{1}{\ln(1/\varepsilon)}\frac{k\hat{\phi}}{\eta}TS,$$

to all log orders, where T and S decouple and are given for large $\check{\tau}$ by (52). In other words,

$$\check{R}^* \sim \frac{k\hat{\phi}}{3\eta\omega} + \frac{1}{\ln(1/\varepsilon)}\frac{k\hat{\phi}\alpha^2\lambda^2\hat{\nu}^2}{252\eta}\check{\tau}^7 \quad \text{as} \quad \check{\tau} \to +\infty.$$

Thus, in order to avoid detailing the intermediate timescale where very little changes (only the leading-order representation of (46) needs modification) we skip straight to the $\check{\tau} \gg \ln^{\frac{1}{7}}(1/\varepsilon)$ behaviour for $\check{R}^*$, and therefore $\check{A}$ also, namely:

$$\check{R}^* \sim \frac{k\hat{\phi}\alpha^2\lambda^2\hat{\nu}^2}{252\eta}\check{\tau}^7, \quad \check{A} \sim \frac{252}{k\hat{\phi}\alpha^2\lambda\hat{\nu}\check{\tau}^6}.$$

Once AgrB, C and D enter the cell membrane, more AIP can be produced and more receptors become available to which these AIPs can bind, allowing the feedback contained within the QS loop fully to take effect, pushing the cells into an up-regulated and virulent state, $P \sim 1$; the system (49) provides a concise representation of the processes that govern the feedback on this timescale, the numbers of AgrB and transmembrane AgrB, C and D in effect being under the control of the mRNA levels (see (50)) rather than themselves during the feedback process. Accordingly, levels of inactive AgrA again decrease as a result of its activation and we see the appearance of the second turning point in A corresponding to this onset of QS (see Figure 11). The timeshift τ_6 (required for the scaling of τ on this timescale, see Table 4) can thus be regarded as the lag time before the autocatalytic reactions have accumulated enough AIP to drive upregulation; it depends upon the rates of transcription, AIP production, AIP binding, AgrA activation and protein dilution, the fundamental processes behind QS.

4.5 Eighth timescale: approach to steady state via protein and mRNA dilution

The seventh timescale is relegated to the Appendix. On the final (eighth) timescale the rescaled equations are

$$\frac{d\bar{M}}{d\bar{\tau}} = \hat{v} - \bar{M} + \varepsilon, \tag{53}$$

$$\varepsilon^2 \frac{d\bar{A}}{d\bar{\tau}} = \lambda \bar{M} - \varepsilon^2 \lambda \bar{A} - \eta \bar{A} \bar{R}^* + \varepsilon \hat{\mu} \eta \bar{A}_P, \tag{54}$$

$$\varepsilon \frac{d\bar{a}}{d\bar{\tau}} = \frac{k\hat{\beta}\hat{\phi}}{\eta} \bar{T} S - \hat{\beta} R \bar{a} + \hat{\beta} \gamma \bar{R}^* - \varepsilon \lambda_a \bar{a}, \tag{55}$$

$$\frac{d\bar{B}}{d\bar{\tau}} = \alpha(\bar{M} - \bar{B}), \tag{56}$$

$$\varepsilon \frac{dS}{d\bar{\tau}} = \lambda(\bar{B} - \varepsilon S) - k\bar{T}S, \tag{57}$$

$$\frac{d\bar{T}}{d\bar{\tau}} = \lambda(\bar{B} - \bar{T}), \tag{58}$$

$$\varepsilon \frac{dR}{d\bar{\tau}} = \lambda \bar{B} - \varepsilon \lambda R - \frac{\eta}{\hat{\phi}} R \bar{a} + \frac{\eta \gamma}{\hat{\phi}} \bar{R}^*, \tag{59}$$

$$\frac{d\bar{R}^*}{d\bar{\tau}} = R\bar{a} - (\lambda + \gamma)\bar{R}^*, \tag{60}$$

$$\frac{d\bar{A}_P}{d\bar{\tau}} = \bar{A}\bar{R}^* - (\lambda + \varepsilon\hat{\mu})\bar{A}_P. \tag{61}$$

At leading order, (57) gives $k\bar{T}S = \lambda\bar{B}$, implying that the leading-order terms of (55) and (59) are equivalent, each yielding (68), i.e. the 'fast' reactions result in transmembrane AgrC (R) and transmembrane AgrD (S) being created and destroyed at the same rates, with a portion of this AgrD being converted into AIP (a). Thus to give a system of independent leading-order equations we take a linear combination of (55), (57) and (59) to eliminate the dominant terms and obtain an additional expression which provides an independent equation on taking the limit ε:

$$\frac{d}{dt}(R - S - \frac{\eta}{\hat{\beta}\hat{\phi}} a) = \frac{\eta \lambda_a}{\hat{\beta}\hat{\phi}} a + \lambda S - \lambda R.$$

The following leading-order expressions then govern the behaviour of the population in this final stage

$$\frac{d\bar{M}}{d\bar{\tau}} = \hat{v} - \bar{M}, \tag{62}$$

$$\frac{d\bar{B}}{d\bar{\tau}} = \alpha(\bar{M} - \bar{B}), \tag{63}$$

$$\frac{d\bar{T}}{d\bar{\tau}} = \lambda(\bar{B} - \bar{T}), \tag{64}$$

$$\frac{d\bar{R}^*}{d\bar{\tau}} = \frac{\hat{\phi}\lambda}{\eta} \bar{B} - \lambda \bar{R}^*, \tag{65}$$

$$\frac{d\bar{A}_P}{d\bar{\tau}} = \frac{\lambda}{\eta} \bar{M} - \lambda \bar{A}_P, \tag{66}$$

$$\frac{d\bar{a}}{d\bar{\tau}} = \frac{\hat{\beta}\hat{\phi}}{\eta}\left(\frac{dR}{d\bar{\tau}} + \lambda R - \frac{dS}{d\bar{\tau}} - \lambda S\right) - \lambda_a a, \tag{67}$$

$$R = \frac{\lambda\hat{\phi}\bar{B} + \eta\gamma\bar{R^*}}{\eta\bar{a}}, \tag{68}$$

$$S = \frac{\lambda\bar{B}}{k\bar{T}}, \tag{69}$$

$$\bar{A} = \frac{\lambda\bar{M}}{\eta\bar{R^*}}, \tag{70}$$

$$P = 1, \tag{71}$$

(67)-(69) can be combined to give the leading-order differential equations for $\bar{a}, S$ or R in terms of $\bar{M}, \bar{B}, \bar{T}$ and $\bar{R^*}$ but we shall not illustrate this here. The following matching conditions hold,

$$\bar{M}(0) = \bar{B}(0) = \bar{T}(0) = \bar{R^*}(0) = \bar{A_P}(0) = \bar{a}(0) = 0. \tag{72}$$

Notice that (71) follows from the seventh timescale, the proportion of up-regulated cells at leading order being given from then onwards as unity. Equations (62)-(71) can be regarded as a minimal model for the QS system of a population which is already in an active state. Moreover, if (62) and (71) were replaced by

$$\frac{d\bar{M}}{d\bar{\tau}} = \hat{v}P - \bar{M} \quad \text{and} \quad \frac{dP}{d\bar{\tau}} = \bar{A_P}(1-P) - uP \tag{73}$$

then this reduced system would be an excellent simplified version of the full model given that it contains the vast majority of reactions which control the *agr* operon at leading order on each timescale. In fact, solving (63)-(70) and (73) numerically, using the original initial conditions for the full model (8) and incorporating the time lag τ_6, really only fails to capture adequately the early dynamics of the TCS because some of the signal transduction reactions are missing.

The system (62)-(70) can be solved sequentially (in the order given), but it is more instructive to illustrate its behaviour numerically - see Figure 12. For each variable we see the asymptotic solution approaching the steady state of the full model. The steady states of the reduced system are thus good approximations to the full steady states. This is particularly useful given that the exact steady states cannot be expressed explicitly; the leading-order terms however give the steady-state ($\tilde{X}$ for each variable X) asymptotics in the form

$$\tilde{P} = 1, \qquad \tilde{M} = \tilde{B} = \tilde{T} = \hat{v}, \qquad \tilde{S} = \frac{\lambda}{k}, \quad \tilde{R^*} = \frac{\hat{\phi}\hat{v}}{\eta}, \quad \tilde{A_P} = \frac{\hat{v}}{\eta}, \quad \tilde{A} = \frac{\lambda}{\hat{\phi}}.$$

$$\tilde{a} = \frac{-\lambda^2\hat{\beta}\hat{\phi} + (\lambda^4\hat{\beta}^2\hat{\phi}^2 + 4\lambda_a\hat{\beta}k^2\lambda\hat{\phi}^2\hat{v}(\lambda+\gamma))^{\frac{1}{2}}}{2\lambda_a\eta k}, \tag{74}$$

$$\tilde{R} = \frac{\lambda^2\hat{\beta}\hat{\phi} + (\lambda^4\hat{\beta}^2\hat{\phi}^2 + 4\lambda_a\hat{\beta}k^2\lambda\hat{\phi}^2\hat{v}(\lambda+\gamma))^{\frac{1}{2}}}{2\lambda\hat{\beta}\hat{\phi}k}.$$

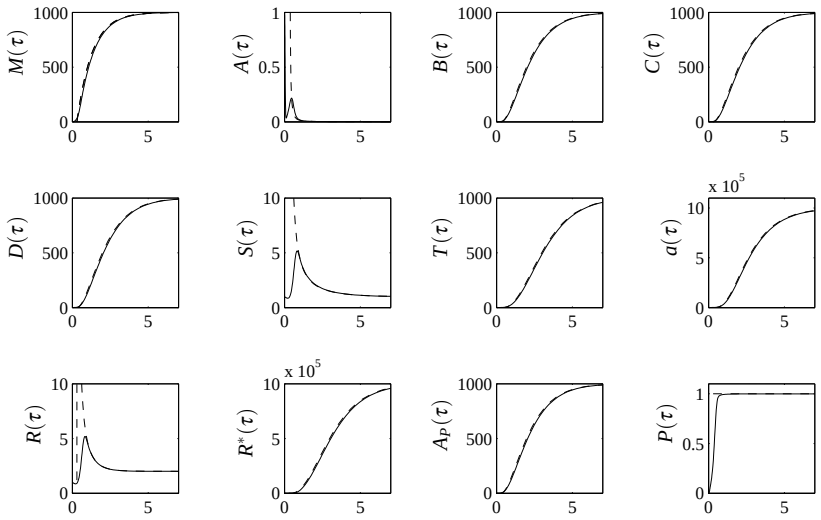

Fig. 12 The solid lines illustrate the numerical solution to the full system for each variable, while the dashed lines represent the corresponding asymptotic approximation on the eighth (final) timescale, on which degradation and dilution lead to the population reaching its up-regulated steady state.

We note that at steady state, the concentration of mRNA (and thus also the remaining variables) is, to leading order, fully under the control of the QS loop, basal transcription being negligible. Since the QS loop takes effect so early on, basal transcription does not in fact come into the leading-order behaviour on any timescale (we are assuming the cells begin in the down-regulated state whereby a small level of proteins have been translated but any AIP has been washed away, and this is sufficient to trigger the start of the QS loop, i.e. basal mRNA transcription has already occurred in order to obtain our initial conditions). In order for basal transcription to occur at leading order we would need much less AIP in the environment of the cells so that the population does not become up-regulated so quickly, for example as in Figure 7. Similarly, housekeeping dephosphorylation of AgrA and dilution of free receptors and inactive AgrA, i.e. the $-\lambda R$ and $-\lambda A$ terms, also never enter at leading order and as such could be neglected from the model altogether (this is because their loss through the activation process dominates). It must be remembered, however, that if the model is extended to include inhibition of the QS loop, say, (see [15]), it is important to retain all those reactions which may play a non-negligible role in suppressed cells.

It is clear from (74) that a key parameter is $\hat{v}$, the ratio of QS-controlled to basal transcription, which affects almost all of the steady state approximations. Notice that

$$\frac{\bar{A_P}}{A+A_P} = \frac{\hat{v}\hat{\phi}}{\lambda\eta+\hat{v}\hat{\phi}} \to 1 \quad \text{as} \quad \hat{v} \to +\infty,$$

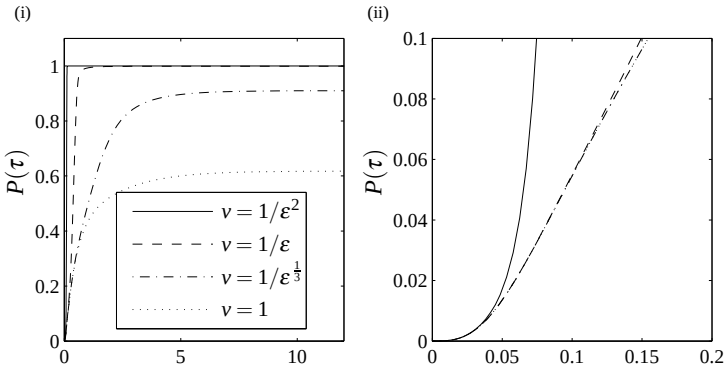

Fig. 13 (i) Numerical solution for $P(\tau)$ from the full model using all parameter values from Table 3 (so that $\varepsilon = 10^{-3}$), except for v, the ratio of the rate of QS-controlled to basal transcription, which is varied here. While altering this ratio ought to affect other parameters (since this ratio is $1/\varepsilon$) we here take all other parameters to be fixed. Decreasing v lowers the proportion of up-regulated cells and the time taken for that proportion to reach an active state is longer, i.e. QS becomes less effective. In (ii) we illustrate these solutions on a shorter timescale in order to demonstrate the lag time before the QS system is fully induced.

and

$$\frac{\bar{R^*}}{\bar{R}+\bar{R^*}} = \frac{2\lambda k\hat{\beta}\hat{\phi}^2\hat{v}}{\lambda^2\eta\hat{\beta}\hat{\phi}+\eta(\lambda^4\hat{\beta}^2\hat{\phi}^2+4\lambda_a\hat{\beta}k^2\lambda\hat{\phi}^2\hat{v}(\lambda+\gamma))^{\frac{1}{2}}+2\lambda k\hat{\beta}\hat{\phi}^2\hat{v}} \to 1$$

as $\hat{v} \to +\infty$, i.e. the AgrA is all active and the receptors are all bound to AIPs in the limit of large $\hat{v}$. Additionally, computing the relevant correction term, we find that

$$\bar{P} \sim 1 - \varepsilon\frac{u\eta}{\hat{v}} \quad \text{as} \quad \varepsilon \to 0.$$

Thus QS-controlled transcription occurring at a much faster rate than basal transcription (i.e. in terms of dimensional parameters $v >> m$) is crucial in ensuring that the QS circuit can function to its full potential. Figure 13 depicts the numerical solution to $P(\tau)$ of the full system for a selection of values of the unscaled nondimensional v. We see that the proportion of active cells decreases significantly with v. If the model is extended to include inhibitor therapy, this correction term is also dependent upon the rate at which inhibitor molecules are introduced to the cells and this is examined further in [15].

Additionally, on considering the time lag τ_6 for the QS activity to take effect:

$$\tau_6 \sim \varepsilon^{-\frac{1}{6}}\left(\frac{\eta}{\lambda\hat{v}}\right)^{\frac{1}{3}}\frac{\ln(1/\varepsilon)}{3},$$

it is evident that the time taken to reach upregulation is reduced as $\hat{v}$ increases. There is a similar, but less sensitive, dependence upon the AIP production rate and rate of AgrA phosphorylation stemming from the time lag τ_3 (see Table 4); increasing either of these will accelerate the cells' process of becoming virulent.

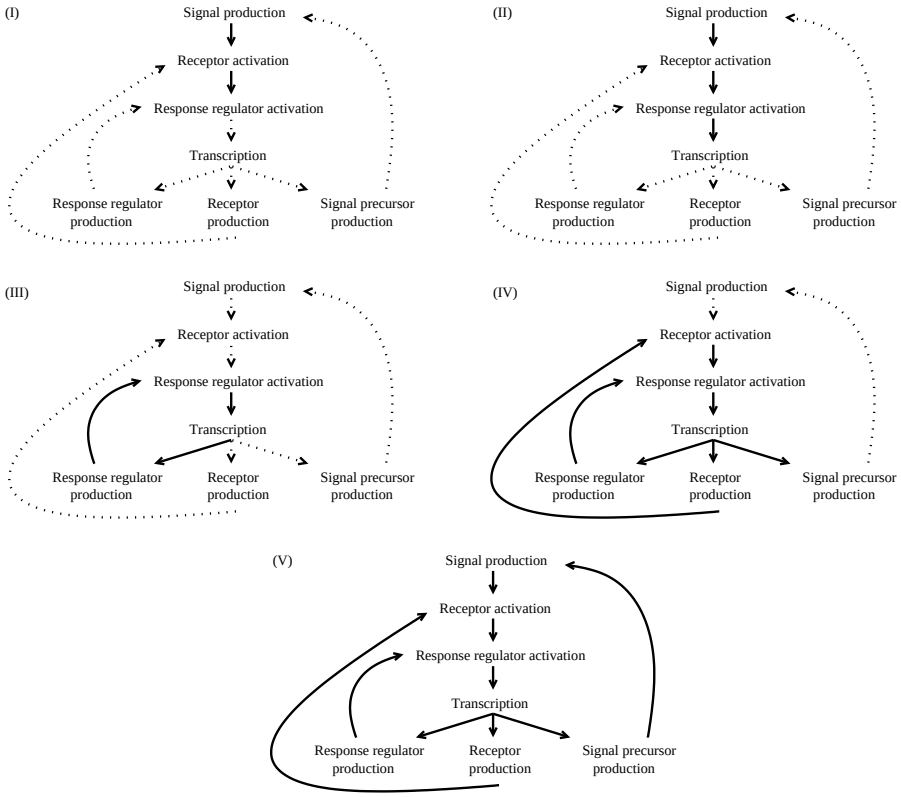

Fig. 14 Here we use the leading-order behaviour on various timescales to present an overview of the stages required for upregulation resulting from a positive feedback loop containing a TCS in which all components of the loop are transcribed from one operon. Solid lines represent leading-order reactions, with dotted lines otherwise. Firstly, (I) the signal is detected by the receptor of the TCS, which then activates the response regulator. This TCS activation induces mRNA transcription, (II). Distinct phases of feedback are then exhibited. Firstly more response regulator is translated so that more can be activated via the TCS, (III). This is followed by increased creation of receptors, which allow more effective signal detection, (IV) and, finally, additional signal precursor is produced, giving more signal and completing the full feedback loop, (V). We have decomposed the response into these stages on the basis of the asymptotic analysis of our system (roughly speaking (I) corresponds to timescale 1, (II) to 2, (III) to 3,4 and 5, (IV) to 6 and 7 and (V) to 8), but they could also be applicable to other such positive feedback loops.

5 Discussion

With the discovery of *agr*-like systems in more and more bacteria (see, for example, [9,21,31,33]), it is becoming increasingly important that this QS system (as illustrated in Figure 1), and why it has evolved to its current form, be understood. We believe that the above asymptotic analysis provides worthwhile insight into the operation of this QS network of which we now highlight a particular aspect. In Figure 14, we demonstrate which of the principal reactions are present at leading order in the various stages of upregulation of the overall feedback loop. [27] provides a discussion as to why a feedback loop might be in place for such a system. However, we

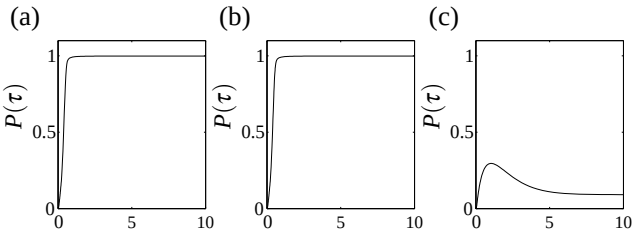

Fig. 15 The numerical solution to $P(t)$ from the nondimensional model of Figure 5 with various sections of the feedback loop removed. In (a) we have removed the feedback into signal production by giving AgrB and AgrD basal production levels at a rate $\alpha = 0.1$ in their respective equations. Similarly, in (b) we have let $\alpha = 0.1$ for AgrC and for AgrA in (c). We see that the only feedback which noticeably affects the proportion of up-regulated cells is the removal of the response regulator sub-loop.

focus our attention on the fact that the feedback loop is divided into three sub-loops, making the *agr* system a rather unusual type of signal amplifier. Such a feedback loop could function by inducing production of a particular component of the system only; however, in the *agr* system each component of the loop - the signal (AIP), receptor (AgrC) and response regulator (AgrA) - is amplified. The asymptotic analysis in effect allows us to separate out each sub-loop and examine each step individually.

Numerical investigations, see Figure 15, indicate that upregulation of AgrA production is the limiting factor in ensuring that the cells reach an up-regulated state (removal of the response regulator feedback sub-loop in (c) results in a significantly lower proportion of up-regulated cells, whereas removal of either of the other two sub-loops in (a) and (b) has a negligible effect upon this number) and this corresponds neatly to our asymptotic analysis: increased AgrA production is present at leading order on an earlier timescale than that of the other proteins. Previous studies assume that the three sub-loops are in place to ensure fast switch-like behaviour in upregulation (see, for example, [17]). However, while this is indeed a plausible argument and has been demonstrated to be the case in mathematical models of other QS systems (see, for example, [2]), the model of [11] produces hysteretic (and hence switch-like) behaviour without the inclusion of all three of these sub-loops. Our analysis suggests that each sub-loop may be in place for distinct reasons: the cells may produce sufficient amounts of AgrA to ensure enough is available for self-activation (it having been demonstrated that it is sufficient to knock-out the *agr* system only in the initial stages of infection to prevent staphylococcal virulence [36], this early use of the AgrA sub-loop is consistent with the idea that the crucial period of *agr* upregulation is this early stage), production of extra AgrC then appearing at leading order for efficient detection of their immediate environment, followed by translation of the additional AgrB and AgrD, which will create AIP, not only for self-activation, but also for activation of other cells in the population. This becomes particularly relevant in the context of a spatially inhomogeneous population whereby some cells will upregulate earlier than others (spatially inhomogeneous models of the *agr* QS system are studied in detail in [15]).

6 Summary

We have presented what we believe to be the first model of the full feedback loop of the *agr* operon in *S. aureus* (previous models of QS in this bacterium have either focused on the TCS alone or not taken into account the intracellular processes). As noted in §1, suppressing the *agr* operon is being examined as a method to treat staphylococcal infection and as such it is important that QS in *S. aureus* be understood as fully as possible. Our analysis demonstrates the step by step processes involved in upregulating the production of secreted virulence factors via the QS loop in *S. aureus*. We see how, if the QS signal molecules are contained within the environment of the bacteria, the feedback loop kicks in rapidly, pushing the cells into an actively virulent state. We have, of course, considered the QS loop in isolation and there are other aspects which could affect the cells' ability to become virulent, e.g. temperature or nutrient supply. A comprehensive representation of the bacteria, in nature or the laboratory, is, given the number and diversity of such features, not within the scope of the type of model analysed here: the current model has the limited goal of describing key aspects of the behaviour of a population of *S. aureus* in a chemostat. This should increase the possibility that parameterisation of the model from experimental work will in due course be possible and many additional factors, such as those mentioned above, are inputs which could be controlled experimentally. The model should also readily be adaptable to describe a growing population of cells, by the addition of a growth term, and other aspects could similarly be incorporated; hence there are many avenues for further investigation and analysis based on the current approach..

This paper derives simpler sub-models which could be used to investigate the *agr* operon further, for example see the first, sixth and final timescales which represent the TCS reactions, the achievement of upregulation and steady-state behaviour respectively. Future publications will examine the effect of suppressing the *agr* operon via a number of methods including using both synthetic inhibitory molecules which compete with AIPs for binding to receptor sites and cross-strain inhibition (strains of *S. aureus* having the ability to naturally interfere with the QS loops of opposing strains), building on the above analysis in order to gain more insight into the advantages and disadvantages of exploiting the staphylococcal QS system for therapeutic gain. The model provides a framework in which to test the sensitivity of various phosphorylation cascades to inhibition and indicate the optimal approaches to manipulating the *agr* operon for therapeutic gain.

In addition to its shedding light on the QS process, we believe the asymptotic analysis we have pursued to be worth presenting in some detail because it provides a mathematical tool of rather general applicability in reducing the complexity of the types of gene and signalling network models that are so prevalent in biological applications (in particular when dimensional parameter values are unknown) and are exemplified by the current application to QS. For instance, equations (63)-(70) and (73) provide an excellent simple substitute for the full model described in Figure 5. The separation of timescales that underpins the success of this approach is similarly widespread but not always exploited. As we show in [15], such techniques extend rather readily to even more complex related systems.

Acknowledgements The authors wish to thank Klaus Winzer for his helpful discussions. S.J. gratefully acknowledges support from the Biotechnology and Biological Sciences Research Council for this work in the form of a studentship, and the other authors that of the Medical Research Council/Engineering and Physical Sciences Research Council. All time-dependent numerical solutions were computed using the ode15s solver in MATLAB v. 7.1 (The MathWorks, Inc.).

A The remaining timescales of the time-dependent asymptotic analysis

We here summarise the timescales which were omitted from the paper.

A.1 Fourth timescale: AgrA translation is balanced by its activation

The rescaled variables on this timescale satisfy

$$\frac{dM^+}{d\tau^+} = \hat{\nu}P^+ - \varepsilon^{\frac{1}{2}}\ln^{\frac{1}{2}}(1/\varepsilon)M^+ + \varepsilon^{\frac{1}{2}}\ln^{-\frac{1}{2}}(1/\varepsilon), \tag{75}$$

$$\ln^{-1}(1/\varepsilon)\frac{dA^+}{d\tau^+} = \lambda M^+ - \varepsilon^{\frac{1}{2}}\ln^{-\frac{1}{2}}(1/\varepsilon)\lambda A^+ - \eta A^+ R^{*+} + \varepsilon\ln^{-1}(1/\varepsilon)\hat{\mu}\eta A_P, \tag{76}$$

$$\varepsilon^{\frac{1}{2}}\ln^{-\frac{1}{2}}(1/\varepsilon)\frac{da^+}{d\tau^+} = \frac{k\hat{\beta}\hat{\phi}}{\eta} - \hat{\beta}a^+ + \varepsilon^{\frac{1}{2}}\ln^{\frac{1}{2}}(1/\varepsilon)\hat{\beta}\gamma R^{*+} - \varepsilon\lambda_a a^+, \tag{77}$$

$$\frac{dR^{*+}}{d\tau^+} = a^+ - \varepsilon^{\frac{1}{2}}\ln^{\frac{1}{2}}(1/\varepsilon)(\lambda+\gamma)R^{*+}, \tag{78}$$

$$\frac{dA_P}{d\tau^+} = \varepsilon^{\frac{1}{2}}\ln^{\frac{3}{2}}(1/\varepsilon)A^+R^{*+} - \varepsilon^{\frac{1}{2}}\ln^{\frac{1}{2}}(1/\varepsilon)(\lambda+\varepsilon\hat{\mu})A_P, \tag{79}$$

$$\frac{dP^+}{d\tau^+} = A_P - \varepsilon^{\frac{1}{2}}\ln^{\frac{1}{2}}(1/\varepsilon)A_P P^+ - \varepsilon^{\frac{1}{2}}\ln^{\frac{1}{2}}(1/\varepsilon)uP^+. \tag{80}$$

Thus to leading order we have

$$\begin{aligned} A_P &= \frac{1}{\eta}, \quad P^+ = \frac{1}{\eta}\left(\tau^+ + \sqrt{\frac{1}{k\hat{\phi}}}\right), \quad M^+ = \frac{\hat{\nu}}{2\eta}\left(\tau^+ + \sqrt{\frac{1}{k\hat{\phi}}}\right)^2, \\ a^+ &= \frac{k\hat{\phi}}{\eta}, \; R^{*+} = \frac{k\hat{\phi}}{\eta}\left(\tau^+ + \sqrt{\frac{1}{k\hat{\phi}}}\right), \; A^+ = \frac{\lambda\hat{\nu}}{2\eta k\hat{\phi}}\left(\tau^+ + \sqrt{\frac{1}{k\hat{\phi}}}\right). \end{aligned} \tag{81}$$

The increasing sequence (from A_P to P and then M) of powers of τ^+ enables us to see what drives each reaction: namely, activator (A_P) increases the proportion of up-regulated cells (P) which, in turn, induces mRNA (M) transcription (this sequence of events begins on the second timescale). Similarly, free AIP concentration (a^+) generates increased levels of AIP-bound receptor (R^{*+}). The combination of AIP-bound receptor and mRNA controls inactive AgrA levels (A), thus completing this section of the feedback loop (remembering that the full loop contains receptor and signal production and these will appear on later timescales). The equations of (81) could be viewed as the large-time behaviour of a TCS forming a positive feedback loop which has an abundance of receptors and signal precursors.

On this timescale, active AgrA is in balance, with Figure 10(ii) illustrating the increase in levels of inactive AgrA (whose translation is now, and is on all the subsequent timescales, balanced by its activation, i.e. $A = \lambda M/\eta R^*$); as we shall now see, this growth of inactive AgrA is subsequently moderated by the translation of all the remaining proteins which results in the activation of more AgrA.

A.2 Fifth timescale: AgrB, C and D translation

While translation of AgrA has already appeared at leading order, we require translation of the remaining proteins, remembering that we have taken $C(\tau), D(\tau) \equiv B(\tau)$. Now (12) no longer applies to B and the equations read

$$\frac{d\check{M}}{d\check{\tau}} = \hat{v}\check{P} - \varepsilon^{\frac{1}{3}}\check{M} + \varepsilon^{\frac{2}{3}}, \tag{82}$$

$$\varepsilon^{\frac{1}{3}}\frac{d\check{A}}{d\check{\tau}} = \lambda\check{M} - \varepsilon^{\frac{2}{3}}\lambda\check{A} - \eta\check{A}\check{R}^* + \varepsilon^{\frac{4}{3}}\hat{\mu}\eta A_P, \tag{83}$$

$$\frac{dB}{d\check{\tau}} = \alpha\check{M} - \varepsilon^{\frac{1}{3}}\alpha B, \tag{84}$$

$$\frac{dS}{d\check{\tau}} = \varepsilon^{\frac{1}{3}}\lambda(B-S) - \varepsilon^{\frac{1}{3}}kTS, \tag{85}$$

$$\frac{dT}{d\check{\tau}} = \varepsilon^{\frac{1}{3}}\lambda(B-T), \tag{86}$$

$$\varepsilon^{\frac{2}{3}}\frac{d\check{a}}{d\check{\tau}} = \frac{k\hat{\beta}\hat{\phi}}{\eta}TS - \hat{\beta}R\check{a} + \varepsilon^{\frac{1}{3}}\hat{\beta}\gamma\check{R}^* - \varepsilon\lambda_a\check{a}, \tag{87}$$

$$\frac{dR}{d\check{\tau}} = \varepsilon^{\frac{1}{3}}\lambda(B-R) - \varepsilon^{\frac{1}{3}}\frac{\eta}{\hat{\phi}}R\check{a} + \varepsilon^{\frac{2}{3}}\frac{\eta\gamma}{\hat{\phi}}\check{R}^*, \tag{88}$$

$$\frac{d\check{R}^*}{d\check{\tau}} = R\check{a} - \varepsilon^{\frac{1}{3}}(\lambda+\gamma)\check{R}^*, \tag{89}$$

$$\frac{dA_P}{d\check{\tau}} = \check{A}\check{R}^* - \varepsilon^{\frac{1}{3}}(\lambda+\varepsilon\hat{\mu})A_P, \tag{90}$$

$$\frac{d\check{P}}{d\check{\tau}} = A_P(1-\varepsilon^{\frac{1}{3}}\check{P}) - \varepsilon^{\frac{1}{3}}u\check{P}. \tag{91}$$

Taking leading-order terms and matching to the fourth timescale gives

$$R(\check{\tau}) = S(\check{\tau}) = T(\check{\tau}) = 1, \qquad \check{a}(\check{\tau}) = \frac{k\hat{\phi}}{\eta}, \qquad \check{R}^* = \frac{k\hat{\phi}}{\eta}\check{\tau},$$

together with the linear system

$$\frac{d\check{M}}{d\check{\tau}} = \hat{v}\check{P}, \qquad \frac{d\check{P}}{d\check{\tau}} = A_P, \qquad \frac{dA_P}{d\check{\tau}} = \frac{\lambda\check{M}}{\eta}; \tag{92}$$

the remaining equations

$$\check{A} = \frac{\lambda\check{M}}{k\hat{\phi}\check{\tau}}, \qquad \frac{dB}{d\check{\tau}} = \alpha\check{M}$$

decouple. The system (92) can be reduced to

$$\frac{d^3\check{P}}{d\check{\tau}^3} - \frac{\lambda\hat{v}}{\eta}\check{P} = 0,$$

with solution

$$\check{P}(\check{\tau}) = c_1 e^{\omega\check{\tau}} + c_2 e^{-\frac{\omega}{2}\check{\tau}}\sin\left(\frac{\sqrt{3}}{2}\omega\check{\tau}\right) + c_3 e^{-\frac{\omega}{2}\check{\tau}}\cos\left(\frac{\sqrt{3}}{2}\omega\check{\tau}\right),$$

where $\omega = (\lambda\hat{v}/\eta)^{\frac{1}{3}}$. Since matching to the previous timescale (in fact, the solutions (81) on the fourth timescale simply correspond to the small $\check{\tau}$ limit of the current ones, but including them separately makes the analysis more transparent) requires

$$\check{P} \sim \frac{1}{\eta}\check{\tau}, \quad \check{P}' \sim \frac{1}{\eta}, \quad \check{P}'' \sim \frac{\lambda\hat{v}}{2\eta^2}\check{\tau}^2 \quad \text{as} \quad \check{\tau}\to 0.$$

Hence $c_1 = 1/3\omega\eta$, $c_2 = \sqrt{3}/3\omega\eta$ and $c_3 = -1/3\omega\eta$, so that

$$\check{P}(\check{\tau}) = \frac{1}{3\omega\eta}\left(e^{\omega\check{\tau}} + \sqrt{3}e^{-\frac{\omega}{2}\check{\tau}}\sin\left(\frac{\sqrt{3}}{2}\omega\check{\tau}\right) - e^{-\frac{\omega}{2}\check{\tau}}\cos\left(\frac{\sqrt{3}}{2}\omega\check{\tau}\right)\right);$$

similarly

$$\check{M}(\check{\tau}) = \frac{\omega}{3\lambda}\left(e^{\omega\check{\tau}} - \sqrt{3}e^{-\frac{\omega}{2}\check{\tau}}\sin\left(\frac{\sqrt{3}}{2}\omega\check{\tau}\right) - e^{-\frac{\omega}{2}\check{\tau}}\cos\left(\frac{\sqrt{3}}{2}\omega\check{\tau}\right)\right),$$
$$\check{A}(\check{\tau}) = \frac{\omega}{3k\hat{\phi}\check{\tau}}\left(e^{\omega\check{\tau}} - \sqrt{3}e^{-\frac{\omega}{2}\check{\tau}}\sin\left(\frac{\sqrt{3}}{2}\omega\check{\tau}\right) - e^{-\frac{\omega}{2}\check{\tau}}\cos\left(\frac{\sqrt{3}}{2}\omega\check{\tau}\right)\right),$$
$$B(\check{\tau}) = \frac{\alpha}{3\lambda}(e^{\omega\check{\tau}} + 2e^{-\frac{\omega}{2}\check{\tau}}\cos\left(\frac{\sqrt{3}}{2}\omega\check{\tau}\right) - 3) + 1,$$
$$A_P(\check{\tau}) = \frac{1}{3\eta}\left(e^{\omega\check{\tau}} + 2e^{-\frac{\omega}{2}\check{\tau}}\cos\left(\frac{\sqrt{3}}{2}\omega\check{\tau}\right)\right).$$

The chain of processes in the *agr* operon continue as translation of all the proteins becomes leading order. On the sixth timescale, once AgrB and AgrD move into the membrane of the cells, the QS loop continues through increased production of AIP. The rate ω of exponential increase is governed by λ, $\hat{v}$ and η. These aspects are all crucial to the success of QS and the exponential blow-up is indicative of the onset of an autoinductive circuit. Thus this fifth timescale represents the onset of QS.

A.3 Seventh timescale: free receptor loss due to AIP binding

This timescale describes how levels of free receptors decrease as more become bound by AIPs. The rescaled equations are

$$\frac{dM'}{d\tau'} = \hat{v}P - \varepsilon^{\frac{1}{4}}M' + \varepsilon, \tag{93}$$
$$\varepsilon\frac{dA'}{d\tau'} = \lambda M' - \varepsilon^{\frac{5}{4}}\lambda A' - \eta A'R^{*\prime} + \varepsilon^{\frac{5}{4}}\hat{\mu}\eta A_P{}', \tag{94}$$
$$\frac{dB'}{d\tau'} = \alpha M' - \varepsilon^{\frac{1}{4}}\alpha B', \tag{95}$$
$$\frac{dR'}{d\tau'} = \lambda B' - \varepsilon^{\frac{1}{4}}\lambda R' - \frac{\eta}{\hat{\phi}}R'a' + \varepsilon^{\frac{1}{4}}\frac{\eta\gamma}{\hat{\phi}}R^{*\prime}, \tag{96}$$
$$\frac{dS'}{d\tau'} = \lambda B' - \varepsilon^{\frac{1}{4}}\lambda S' - kT'S', \tag{97}$$
$$\frac{dT'}{d\tau'} = \lambda B' - \varepsilon^{\frac{1}{4}}\lambda T', \tag{98}$$
$$\varepsilon\frac{da'}{d\tau'} = \frac{k\hat{\beta}\hat{\phi}}{\eta}T'S' - \hat{\beta}R'a' + \varepsilon^{\frac{1}{4}}\hat{\beta}\gamma R^{*\prime} - \varepsilon^{\frac{5}{4}}\lambda_a a', \tag{99}$$
$$\frac{dR^{*\prime}}{d\tau'} = R'a' - \varepsilon^{\frac{1}{4}}(\lambda+\gamma)R^{*\prime}, \tag{100}$$
$$\frac{dA_P{}'}{d\tau'} = A'R^{*\prime} - \varepsilon^{\frac{1}{4}}(\lambda+\varepsilon\hat{\mu})A_P{}', \tag{101}$$
$$\varepsilon^{\frac{1}{4}}\frac{dP}{d\tau'} = A_P{}'(1-P) - \varepsilon^{\frac{1}{2}}uP. \tag{102}$$

The leading-order solutions are

$$P = 1, \quad M' = \hat{v}\tau', \quad B' = \frac{\alpha\hat{v}}{2}\tau'^2, \quad T' = \frac{\alpha\lambda\hat{v}}{6}\tau'^3, \quad a' = \frac{\alpha k\hat{\phi}\lambda\hat{v}}{6\eta}\tau'^3, \quad A_P{}' = \frac{\lambda\hat{v}}{2\eta}\tau'^2,$$

along with the long-term behaviour,

$$S', R' \sim \frac{3}{k\tau'}, \qquad R^{*\prime} \sim \frac{\hat{\phi}\alpha\lambda\hat{v}}{6\eta}\tau'^3, \qquad A' \sim \frac{6}{\hat{\phi}\alpha\tau'^2},$$

as $\tau' \to \infty$.

Now that the cells have reached an up-regulated state, the QS loop continues, but the level of free receptors and transmembrane AgrD begins to decrease as more receptors become bound by AIP, continuing to activate the cells and more AIPs are produced. This decrease is evident in the numerical solutions shown in Figure 6 and corresponds with the sharp decrease following the maximum values of $R(\tau)$ (receptor proteins) and $S(\tau)$ (transmembrane AgrD). Notice that, despite being governed by very different terms at

leading order, these two variables behave identically until this timescale (we will see on the final timescale that their steady state behaviour will differ). This is due to the fact that the numbers of receptors and AIP are in balance with the two proteins required to produce the signal (AgrB and AgrD) each being ultimately determined by mRNA levels.

References

1. Anguige K., King J.R., Ward J.P.: Modelling antibiotic- and anti-quorum sensing treatment of a spatially-structured *Pseudomonas aeruginosa* population. J. Math. Biol. **51**, 557–594 (2005)
2. Anguige K., King J.R., Ward J.P., Williams P.: Mathematical modelling of therapies targeted at bacterial quorum sensing. Math. Biosci. **192**, 39–83 (2004)
3. Cámara M., Williams P., Hardman, A.: Controlling infection by tuning in and turning down the volume of bacterial small-talk. Lancet Infect. Dis. **2**, 667–676 (2002)
4. Chan W.C., Coyle B.J., Williams P.: Virulence regulation and quorum sensing in staphylococcal infections: competitive AgrC antagonists as quorum sensing inhibitors. J. Med. Chem. **47**, 4633–4641 (2004)
5. Cheung A.L.: Global regulation of virulence determinants in *Staphylococcus aureus*. In: Honeyman A.L., Friedman H., Bendinelli M. (ed.) Staphylococcus aureus Infection and Disease, pp. 295–322. Kluwer Academic/Plenum Publishers (2001)
6. Dockery J.D., Keener J.P.: A mathematical model for quorum sensing in *Pseudomonas Aeruginosa*. Bull. Math. Biol. **63**, 95–116 (2001)
7. Fagerlind M.G., Rice S.A., Nilsson P., Harlén M., James S., Charlton T., Kjelleberg S.: The role of regulators in the expression of quorum-sensing signals in *Pseudomonas aeruginosa*. J. Mol. Microbiol. Biotechnol. **6**, 88–100 (2003)
8. Finch R.: Gram-positive infections: lessons learnt and novel solutions. Clin. Microbiol. Infec. **12**, 3–8 (2006)
9. Fujii T., Ingham C., Nakayama J., Beerthuyzen M., Kunuki R., Molenaar D., Sturme M., Vaughan E., Kleerebezem M., de Vos W.: Two homologous agr-like quorum-sensing systems cooperatively control adherence, cell morphology, and cell viability properties in *Lactobacillus plantarum* WCFS1. J. Bacteriol. **190**, 7655–7665 (2009)
10. George E.A., Muir T.W.: Molecular mechanisms of *agr* quorum sensing in virulent staphylococci. ChemBioChem. **8**, 847–855 (2007)
11. Gustafsson E., Nilsson P., Karlsson S., Arvidson S.: Characterizing the dynamics of the quorum-sensing system in *Staphylococcus aureus*. J. Mol. Microbiol. Biotechnol. **8**, 232–242 (2004)
12. Hense B.A., Kuttler C., Müller J., Rothballer M., Hartmann A., Kreft J.: Does efficiency sensing unify diffusion and quorum sensing? Nature Rev. Mirobiol. **5**, 230–239 (2007)
13. Hiramatsu K., Aritaka N., Hanaki H., Kawasaki S., Hosoda Y., Hori S., Fukuchi Y., Kobayashi I.: Dissemination in Japanese hospitals of strains of *Staphylococcus aureus* heterogeneously resistant to vancomycin. Lancet **350**, 1670–1673 (1997)
14. Jabbari S.: *Computational modelling of quorum sensing in Staphylococcus aureus* (2004). Qualifying dissertation, University of Nottingham
15. Jabbari S.: Mathematical modelling of quorum sensing and its inhibition in *Staphylococcus aureus*. Ph.D. thesis, University of Nottingham, UK (2007)
16. James S., Nilsson P., James G., Kjelleberg S., Fagerström T.: Luminescence control in the marine bacterium *Vibrio fischeri*: an analysis of the dynamics of *lux* regulation. J. Mol. Biol. **296**, 1127–1137 (2000)
17. Ji G., Beavis R.C., Novick R.P.: Cell density control of staphylococcal virulence mediated by an octapeptide pheromone. Proc. Natl. Acad. Sci. USA **92**, 12,055–12,059 (1995)
18. Kevorkian J., Cole J.D.: Perturbation methods in applied mathematics. Springer-Verlag (1981)
19. Koenig R.L., Ray J.L., Maleki S.J., Smeltzer M.S., Hurlburt B.K.: *Staphylococcus aureus* AgrA binding to the RNAIII-*agr* regulatory region. J. Bacteriol. **186**, 7549–7555 (2004)
20. Koerber A.J., King J.R., Williams P.: Deterministic and stochastic modelling of endosome escape by *Staphylococcus aureus*: "quorum sensing" by a single bacterium. J. Math. Biol. **50**, 440–488 (2005)
21. Lazazzera B.A., Palmer T., Quisel J., Grossman A.D.: Cell density control of gene expression and development in *Bacillus subtilis*. In: Dunny G.M., Winans S.C. (ed.) Cell-cell signaling in bacteria, pp. 27–46. American Society for Microbiology (1999)

22. Mayville P., Ji G., Beavis R., Yang H., Goger M., Novick R.P., Muir T.W.: Structure-activity analysis of synthetic autoinducing thiolactone peptides from *Staphylococcus aureus* responsible for virulence. Proc. Natl. Acad. Sci. USA **96**, 1218–1223 (1999)
23. McDowell P., Affas Z., Reynolds C., Holden M.T.G., Wood S.J., Saint S., Cockayne A., Hill P.J., Dodd C.E.R., Bycroft B.W., Chan W.C., Williams P.: Structure, activity and evolution of the group I thiolactone peptide quorum-sensing system of *Staphylococcus aureus*. Mol. Microbiol. **41**, 503–512 (2001)
24. Miller M.B., Bassler B.L.: Quorum sensing in bacteria. Annu. Rev. Microbiol. **55**, 165–199 (2001)
25. Müller J., Kuttler C., Hense B.A., Rothballer M., Hartmann A.: Cell-cell communication by quorum sensing and dimension-reduction. J. Math. Biol. **53**, 672–702 (2006)
26. Novick R.P.: Autoinduction and signal transduction in the regulation of staphylococcal virulence. Mol. Microbiol. **48**, 1429–1449 (2003)
27. Novick R.P., Geisinger E.: Quorum sensing in Staphylococci. Annu. Rev. Genet. **42**, 541–64 (2008)
28. Otto M.: Quorum-sensing control in staphylococci - a target for antimicrobial drug therapy? FEMS Microbiol. Lett. **241**, 135–141 (2004)
29. Pearson H.: 'Superbug' hurdles key drug barrier. Nature **418**, 469 (2002)
30. Redfield R.J.: Is quorum sensing a side effect of diffusion sensing? Trends Microbiol. **10**, 365–370 (2002)
31. Riedel C.U., Monk I.R., Casey P.G., Waidmann M.S., Gahan C.G.M., Hill C.: AgrD-dependent quorum sensing affects biofilm formation, invasion, virulence and global gene expression profiles in *Listeria monocytogenes*. Mol. Microbiol. **71**, 1177–1189 (2009)
32. Salmond G.P.C., Bycroft B.W., Stewart G.S.A.B., Williams P.: The bacterial 'enigma': cracking the code of cell-cell communication. Mol. Microbiol. **16**, 615–624 (1995)
33. Sebaihia M., Peck M.W., Minton N.P. *et al.*: Genome sequence of a proteolytic (Group I) *Clostridium botulinum* strain Hall A and comparative analysis of the clostridial genomes. Genome Res. **17**, 1082–1092 (2007)
34. Ward J.P., King J.R., Koerber A.J., Williams P., Croft J.M., Sockett R.E.: Mathematical modelling of quorum sensing in bacteria. IMA J. Math. Appl. Med. **18**, 263–292 (2001)
35. Wilson M., McNab R., Henderson B.: Bacterial disease mechanisms, an introduction to cellular microbiology. Cambridge University Press (2002)
36. Wright III J.S., Jin R., Novick R.P.: Transient interference with staphylococcal quorum sensing blocks abscess formation. Proc. Natl. Acad. Sci. USA **102**, 1691–1696 (2005)
37. Yarwood J.M., Schlievert P.M.: Quorum sensing in *Staphylococcus* infections. J. Clin. Invest. **112**, 1620–1625 (2003)